CCFE-PR(16)66

I. Rovelli, S.L. Dudarev and A.P. Sutton

Non-local Model for Diffusion-Mediated Dislocation Climb and Cavity Growth

Enquiries about copyright and reproduction should in the first instance be addressed to the Culham Publications Officer, Culham Centre for Fusion Energy (CCFE), K1/0/83, Culham Science Centre, Abingdon, Oxfordshire, OX14 3DB, UK. The United Kingdom Atomic Energy Authority is the copyright holder.

Non-local Model for Diffusion-Mediated Dislocation Climb and Cavity Growth

I. Rovelli[a,b], S.L. Dudarev[b], A.P. Sutton[a]

[a]Department of Physics, Imperial College London, Exhibition Road, London SW7 2AZ, United Kingdom
[b]Culham Centre for Fusion Energy, UK Atomic Energy Authority, Abingdon, Oxfordshire OX14 3DB, United Kingdom

Further reproduction distribution of this paper is subject to the journal publication rules.

Non-local Model for Diffusion-Mediated Dislocation Climb and Cavity Growth

I. Rovelli[a,b,*], S.L. Dudarev[b], A.P. Sutton[a]

[a] *Department of Physics, Imperial College London, Exhibition Road, London SW7 2AZ, United Kingdom*
[b] *Culham Centre for Fusion Energy, UK Atomic Energy Authority, Abingdon, Oxfordshire OX14 3DB, United Kingdom*

Abstract

To design efficient thermal recovery procedures for structural materials in fusion energy applications it is important to characterise quantitatively the annealing timescales of radiation-induced defect clusters. With this goal in mind, we present an extension of the Green's function formulation of Gu et al. [1] for the climb of curved dislocations, to include in the same framework the evaporation and growth of cavities and the effects of free surfaces. This paper focuses on the mathematical foundations of the model, which makes use of boundary integral equations [2] to solve the steady-state vacancy diffusion problem. Numerical results are also presented in the simplified case of a dilute configuration of prismatic dislocation loops and spherical cavities in a finite-size medium, which show good agreement with experimental data on defect annealing in ion-irradiated tungsten [3].

Keywords: Bulk Diffusion, Dislocations, Voids and Inclusions, Boundary Integral Equations

1. Introduction

Achieving energy production via nuclear fusion reactors is one of the most technologically demanding engineering projects of our time. Proposed materials for plasma-facing-components (PFCs) in tokamak reactors include ferritic-martensitic steels, tungsten, copper alloys, vanadium alloys, and titanium alloys. The primary causes of damage to PFCs are high energy neutrons and ions produced in the fusion plasma [4]. The momentum transferred from the impacting neutrons displaces atoms from their equilibrium positions, generating free vacancies and self-interstitials, which coalesce into nanometre-size defect clusters, degrading the mechanical, thermal and electrical properties of PFCs. Experimental characterisations [5, 3, 6, 7, 8] have identified vacancy and interstitial prismatic dislocation loops, and voids as the most commonly occurring defect clusters following irradiation by high-energy particles. Furthermore, it has been shown that post-irradiation annealing enables properties of the material to recover, at least to some extent, which is a promising route for the maintenance of structural materials in fission and fusion reactors. This highlights the need for a modelling framework able to predict the time-scales of defect coarsening and annealing, while taking into account the complex collective interactions between defect clusters.

We begin with a brief overview of modelling techniques for radiation damage production and the annealing of irradiation defects. We focus on a recent model that accounts for non-local effects mediated by the vacancy field to calculate the climb rates of dislocations. We then present a generalisation of this model, treating cavities and grain boundaries in the same framework. Finally, we present some preliminary simulations of the combined annealing of cavities and dislocation loops in the dilute limit. We apply these ideas to tungsten, which is increasingly regarded as a preferred candidate material for PFCs [9] and also has the computational advantage of having almost isotropic elastic properties.

1.1. Overview of available theoretical modelling

Molecular dynamics (MD) simulations have been widely used to simulate the effect of high-energy particles impacting on a material [10]. Although they provide insight into the formation of collision cascades,

*Corresponding author
Email address: ir1014@ic.ac.uk (I. Rovelli)

MD simulations with classical potentials can capture processes only with timescales of less than 1 μs. Depending on the barriers to point defect migration in relation to k_BT, coarsening of radiation defect microstructures can require seconds to hours.
Rate theory models for microstructure evolution [11] and inhomogeneous cavity growth [12] under irradiation conditions have successfully predicted the timescales of radiation defect generation and the evolution of their distributions. A disadvantage of such models is that they include long-range elastic interactions only through mean-field bias factors, and thus are unable to address the evolution of experimentally observed complex heterogeneous microstructures of defects that originate from elastic interactions. In-situ TEM characterisation of irradiated metals have shown that dislocation loops perform one-dimensional stochastic Brownian motion [13], which are affected by elastic interactions when the loop density is high. This phenomenon and its consequences for the spatial ordering of dislocation loops have been investigated with Langevin dynamics simulations employing stochastic equations for loop motion [14, 15]. In particular, it has been proposed [15] that the combined effect of Brownian motion and elastic interactions between loops is responsible for the formation of dislocation rafts in irradiated materials.
To take into account more complex interactions between dislocations during coarsening, such as loop coalescence (observed for instance in [3]), Discrete Dislocation Dynamics (DDD) simulations are required. In DDD, dislocation lines are discretised in straight segments defined by a set of nodes. At each simulation step the elastic field generated by each segment is calculated and the position of each node is updated according the force acting on each segment and an assumed relationship between velocity and force. This enables the analysis of more complex dislocation structures. Each segment is characterised by a Burgers vector $\mathbf{b}$ and a local dislocation line direction $\boldsymbol{\xi}$, and the force acting on it is determined by the Peach-Koehler formula:

$$\mathbf{f}_{\mathrm{PK}} = (\boldsymbol{\sigma} \cdot \mathbf{b}) \times \boldsymbol{\xi} \tag{1}$$

where $\boldsymbol{\sigma}$ is the Cauchy stress tensor. For a dislocation which is not pure screw the Peach-Koehler force can be decomposed into a *climb* component $\mathbf{f}_{\mathrm{cl}}$, acting in the direction defined by $\boldsymbol{\xi} \times \mathbf{b}$, and a *glide* component $\mathbf{f}_{\mathrm{gl}}$, parallel to $\boldsymbol{\xi} \times (\boldsymbol{\xi} \times \mathbf{b})$.
In the majority of DDD codes [16, 17, 18, 19], node velocities are assumed to obey a mobility law of the form:

$$\mathbf{v} = \mathbf{v}_{\mathrm{gl}} + \mathbf{v}_{\mathrm{cl}} = \mathbf{M}_{\mathrm{gl}} \cdot \mathbf{f}_{\mathrm{gl}} + \mathbf{M}_{\mathrm{cl}} \cdot \mathbf{f}_{\mathrm{cl}} \tag{2}$$

where $\mathbf{M}_{\mathrm{gl}}$ and $\mathbf{M}_{\mathrm{cl}}$ are empirical, material dependent, mobility tensors. However, we stress that climb motion is a non-conservative process involving the diffusion of point defects to (or from) the dislocation core. The climb velocity of a dislocation segment depends on the availability of point defects in its neighbourhood, which in turn is determined by the total distribution of point defect sinks (or sources) in the whole medium. The mobility law of eq.2 is therefore inaccurate when treating systems with high densities of sinks, such as when discussing the combined coarsening of dislocation loops and cavities.

1.1.1. Non-local modelling of dislocation climb

In a recent paper by Gu et al. [1] a new continuum model for dislocation climb was proposed. The model is based on the Green's function formalism and explicitly takes into account non-local interactions between dislocation segments mediated through the vacancy field.
Consider a general infinite material containing an arbitrary number of dislocations, of arbitrary character and shape, and let Γ denote the union of all dislocation segments. Assuming that vacancies are the only type of mobile point defects, and neglecting pipe diffusion, the local vacancy concentration per atomic site $c(\mathbf{x}, t)$ (which is a dimensionless quantity), obeys the diffusion equation:

$$\frac{\partial c(\mathbf{x}, t)}{\partial t} = -\Omega \nabla \cdot \mathbf{J}(\mathbf{x}, t) - \Omega I(\mathbf{x}, t) \delta(\Gamma) \tag{3}$$

where $\mathbf{J}$ is the local vacancy flux, I is the local vacancy current flowing towards a dislocation segment, per unit length, and Ω is the vacancy volume. The generalised delta-function on Γ has the dimensions of inverse square length and is defined such that, for every test function $f(\mathbf{x}) \in C^{\infty}(\mathbb{R}^3)$, we have:

$$\int_{\mathbb{R}^3} \delta[\Gamma] f(\mathbf{x}) dV = \int_{\Gamma} f(\mathbf{x}) dl \tag{4}$$

The local vacancy flux is given by:

$$\mathbf{J}(\mathbf{x},t) = -\frac{D_v c(\mathbf{x},t)}{\Omega k_B T}\nabla\mu_v(\mathbf{x},t) \tag{5}$$

where D_v is the vacancy diffusion coefficient, μ_v is the local vacancy chemical potential, k_B is Boltzmann's constant and T is absolute temperature. The vacancy chemical potential, provided that $c \ll 1$ and that the crystal is cubic, has the form:

$$\mu_v(\mathbf{x},t) = k_B T \log\frac{c(\mathbf{x},t)}{c_0} - P(\mathbf{x},t)\Omega_r \tag{6}$$

where P is the local hydrostatic pressure, Ω_r is the vacancy relaxation volume [20, 21], defined as the difference between the volume of a relaxed crystal containing a single vacancy and the perfect reference crystal, and c_0 is the equilibrium vacancy concentration:

$$c_0 = \exp\left(-\frac{E_v}{k_B T}\right) \tag{7}$$

with E_v the vacancy formation energy in the bulk. By substituting the expression for $\mathbf{J}$ we obtain:

$$\frac{\partial c(\mathbf{x},t)}{\partial t} = \nabla\cdot\left[D_v\nabla c(\mathbf{x},t) + \frac{D_v\Omega_r}{k_B T}c(\mathbf{x},t)\nabla P(\mathbf{x},t)\right] - I(\mathbf{x},t)\Omega\delta(\Gamma) \tag{8}$$

The term proportional to the hydrostatic pressure can be ignored since the magnitude of the stresses outside the dislocation core region are generally small. In that case the equilibrium vacancy concentration and the vacancy diffusion coefficient can be regarded as constant. Then we have:

$$\frac{\partial c(\mathbf{x},t)}{\partial t} = D_v\nabla^2 c(\mathbf{x},t) - I(\mathbf{x},t)\Omega\delta(\Gamma) \tag{9}$$

If the density of vacancy sinks, i.e. dislocation segments, is sufficiently high, the vacancy field can be assumed to equilibrate on much shorter timescales than those linked to climb motion. The vacancy concentration can then be considered adiabiatic[1] with respect to Γ, leading to the steady-state (Poisson) equation:

$$D_v\nabla^2 c = I\Omega\delta(\Gamma) \tag{10}$$

The vacancy current I is related to the dislocation climb velocity v_{cl} as follows:

$$I\Omega = b_e v_{\mathrm{cl}} \tag{11}$$

where $b_e = |\boldsymbol{\xi}\times\mathbf{b}|$ is the edge component of the Burgers vector. By imposing a fixed concentration far from Γ, the following boundary value problem is defined:

$$\begin{cases} D_v\nabla^2 c = b_e v_{\mathrm{cl}}\delta(\Gamma) \\ c(r\to\infty) = c_\infty \end{cases} \tag{12}$$

Employing the Green's function formalism, the solution can be written as follows:

$$c(\mathbf{x}) = \int_\Gamma G_0(\mathbf{x}-\mathbf{x}')b_e(\mathbf{x}')v_{\mathrm{cl}}(\mathbf{x}')dl' + c_\infty = -\frac{1}{4\pi D_v}\int_\Gamma \frac{b_e(\mathbf{x}')v_{\mathrm{cl}}(\mathbf{x}')}{|\mathbf{x}-\mathbf{x}'|}dl' + c_\infty \tag{13}$$

where dl' is the line element over Γ, and $G_0(\mathbf{x}) = -1/(4\pi D_v|\mathbf{x}|)$ is the solution of Poisson's equation in an infinite medium for a point source at the origin: $D_v\nabla^2 G_0(\mathbf{x}) = \delta(\mathbf{x})$.
The adiabatic assumption implies that local equilibrium must exist between each dislocation segment and the surrounding vacancy field. This can be cast in a thermodynamic framework by requiring that there is no net change in free energy related to the absorption (or emission) of a vacancy by (from) a dislocation line. Thus, consider a straight dislocation that climbs a distance δs in the direction of $\boldsymbol{\xi}\times\mathbf{b}$, under the in-

[1] This assumption is checked quantitatively in section 3.4

fluence of an elastic climb force $f_{\rm cl} = \mathbf{f}_{\rm PK} \cdot (\boldsymbol{\xi} \times \mathbf{b}/b_e)$. We note that by this convention $f_{\rm cl}$ is positive when the relative vector force points in the direction of climb due to the *absorption* of a vacancy. The climb process requires the absorption by the dislocation of a number of vacancies n per unit length L given by:

$$\frac{n}{L} = \frac{\delta s \, b_e}{\Omega} \tag{14}$$

If c_Δ is the vacancy concentration at the boundary with the dislocation core, the local vacancy chemical potential is:

$$\mu_{\rm v} = k_B T \ln \frac{c_\Delta}{c_0} \tag{15}$$

The free energy change δF due to climb motion is therefore given by:

$$\delta F = -L \frac{\delta s \, b_e}{\Omega} k_B T \ln \frac{c_\Delta}{c_0} - L \delta s f_{\rm cl} \tag{16}$$

Now consider an arbitrarily shaped dislocation Γ. In this case the quantities δs, $f_{\rm cl}$ and c_Δ are, in general, not constant, but depend on the position along the dislocation. The total change in free energy due to climb motion then becomes:

$$\delta F = \int_\Gamma dl \left[-\frac{b_e(\mathbf{x})}{\Omega} k_B T \ln \frac{c_\Delta(\mathbf{x})}{c_0} - f_{\rm cl}(\mathbf{x}) + \kappa(\mathbf{x}) E_c \right] \delta s(\mathbf{x}) \tag{17}$$

where $\kappa(\mathbf{x})$ is the local line curvature in the climb direction and E_c is the core contribution to the dislocation line tension. The assumption of *local* thermodynamic equilibrium leads to the relationship:

$$-\frac{b_e(\mathbf{x})}{\Omega} k_B T \ln \frac{c_\Delta(\mathbf{x})}{c_0} - f_{\rm cl}(\mathbf{x}) + \kappa(\mathbf{x}) E_c = 0 \tag{18}$$

which, in turn, determines the boundary condition for $c_\Delta(\mathbf{x})$:

$$c_\Delta(\mathbf{x}) = c_0 \exp \left[-\frac{[f_{\rm cl}(\mathbf{x}) - \kappa(\mathbf{x}) E_c] \, \Omega}{b_e(\mathbf{x}) k_B T} \right] \tag{19}$$

It is reasonable to include the term $\kappa(\mathbf{x}) E_c$ in $f_{\rm cl}$. Eq.13 can then be recast as:

$$-\frac{1}{4\pi D_v} \int_\Gamma \frac{b_e(\mathbf{x}') v_{\rm cl}(\mathbf{x}')}{|\mathbf{x} - \mathbf{x}'|} dl' + c_\infty = c_0 \exp \left[-\frac{f_{\rm cl}(\mathbf{x}) \, \Omega}{b_e(\mathbf{x}) k_B T} \right] \qquad \forall \mathbf{x} \in \Gamma \tag{20}$$

which is an implicit integral equation to be solved for the unknown function $v_{\rm cl}(x, y, z)$. In a discrete dislocation dynamics framework, eq.20 can be solved numerically by evaluating the right hand side on each discretisation node and by expressing the left hand side as a function of the climb velocities of each node, using a quadrature formula. This gives the matrix equation:

$$\sum_j a_{ij} v_{\rm cl}^j = c_\infty - c_0 \, \exp \left[-\frac{f_{\rm cl}^i \, \Omega}{b_e^i k_B T} \right] \tag{21}$$

where $v_{\rm cl}^i$, $f_{\rm cl}^i$ and ${b_e}^i$ respectively denote the climb velocity, the climb force and the edge component of the Burgers vector on the i-th node, and a_{ij} is a matrix of quadrature coefficients.
In contrast to using an empirical expression like eq.2, in this model the climb velocity is calculated explicitly using the vacancy concentrations in local equilibrium with each dislocation segment. The calculated corrections to $v_{\rm cl}$ have been shown [1] to be particularly important where multiple vacancy sinks are closely packed together, as in the case of the annealing of radiation defects.
One of the shortcomings of this treatment for investigating the evolution of radiation defects is that it does not take into account the effect of sinks such as cavities, external free surfaces, and grain boundaries. In principle surface sinks could be included but the Green's function would then no longer be that of the infinite medium, and it would have to be recomputed as the microstructure evolved. As previously mentioned, a significant fraction of radiation-induced defects are cavities, which also act as vacancy sinks. A satisfactory model for the annealing of radiation damage microstructures must treat all these defects in the same framework and predict their rates of growth and shrinkage.

In the following section we will derive a more general model that aims to achieve this goal.

2. Non-local model for cavity annealing

Consider a singe-crystalline material region V containing N cavities and bounded by an external surface $\partial V = S_e$. We limit ourselves to the case where irradiation from high energy particles and the consequent generation of point defects has already stopped, leaving as a result a population of cavities and dislocation loops, both of interstitial and vacancy type. Since self-interstitials are typically characterized by much higher formation energies and much lower migration barriers than vacancies [22], we can assume that the population of mobile point defects consists only of vacancies. In particular, it has been suggested [5] from experimental data that interstitials would diffuse to grain boundaries over much shorter timescales than those related to the macroscopic evolution of defect clusters.
In order to streamline the presentation we will first focus on the evolution of cavities. We will then discuss prismatic dislocation loops and show how our modelling framework recovers the Green's function formulation of Gu et al. [1]

2.1. Problem definition

Let Σ_i be the surface of the i-th cavity, then the vacancy concentration in the medium is governed by the equation:

$$\frac{\partial c(\mathbf{x},t)}{\partial t} = D_v \nabla^2 c(\mathbf{x},t) - \Omega J_n(\mathbf{x},t) \left[\sum_{i=1}^{N} \delta[\Sigma_i(t)] + \delta\left[S_e(t)\right] \right] \tag{22}$$

where $c(\mathbf{x},t)$ is the (dimensionless) vacancy concentration per atomic site, D_v is the vacancy diffusion coefficient and J_n is the vacancy current normal to a free surface.
The generalised delta-function on a surface has the dimensions of length^{-1} and, similarly to eq.4, is defined as:

$$\int_{\mathbb{R}^3} \delta[\Sigma] f(\mathbf{x}) dV = \int_{\Sigma} f(\mathbf{x}) dS \tag{23}$$

Assuming again that vacancy equilibration is much faster than the rate of growth of cavities, we can use the steady-state approximation:

$$D_v \nabla^2 c(\mathbf{x}) = \Omega J_n(\mathbf{x}) \left[\sum_{i=1}^{N} \delta[\Sigma_i(t)] + \delta\left[S_e(t)\right] \right] \tag{24}$$

A formal solution of the above equation has the form:

$$c(\mathbf{x}) = \Omega \left[\sum_{i=1}^{N} \int_{\Sigma_i} G(\mathbf{x},\mathbf{x}') J_n(\mathbf{x}') dS' + \int_{S_e} G(\mathbf{x},\mathbf{x}') J_n(\mathbf{x}') dS' \right] \tag{25}$$

which is a naive extension of the treatment of dislocation climb given by Gu et al. [1]. In this case, however, $G(\mathbf{x},\mathbf{x}')$ is *not* the free space Green's function $G_0(\mathbf{x},\mathbf{x}')$, but instead it depends on the position, shape and size of each free surface in the material portion under investigation. Calculating the correct $G(\mathbf{x},\mathbf{x}')$ for every given configuration is a cumbersome, computationally unfeasible task.
An alternative formulation is therefore needed in order to treat cavities and general free surfaces. In the following section we will make use of Kirchhoff integral representation in order to obtain expressions containing only $G_0(\mathbf{x},\mathbf{x}')$.

2.2. Kirchhoff integral representation

Let $V \in \mathbb{R}^3$ be an arbitrary connected (but not necessarily *simply* connected) region in space and let $S = \partial V$. We can write the identity:

$$\nabla' \cdot [c(\mathbf{x}')\nabla' G_0(\mathbf{x},\mathbf{x}')] - \nabla' \cdot [G_0(\mathbf{x},\mathbf{x}')\nabla' c(\mathbf{x}')] = c(\mathbf{x}')\nabla'^2 G_0(\mathbf{x},\mathbf{x}') - G_0(\mathbf{x},\mathbf{x}')\nabla'^2 c(\mathbf{x}') \tag{26}$$

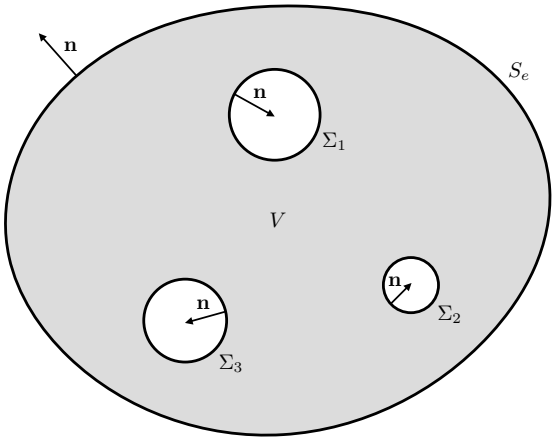

Figure 1: Schematic diagram of the system under consideration, highlighting the convention for surface normals. The region is V is shaded in grey.

where G_0 is the free space Green's function of the steady-state diffusion problem, and primed derivatives are considered to act only on primed variables. Integrating the left hand term over V and applying Gauss' theorem:

$$\int_V \nabla' \cdot [c(\mathbf{x}')\nabla' G_0(\mathbf{x},\mathbf{x}') - G_0(\mathbf{x},\mathbf{x}')\nabla' c(\mathbf{x}')]\, dV' =$$

$$= \int_S [c(\mathbf{x}')\nabla' G_0(\mathbf{x},\mathbf{x}') - G_0(\mathbf{x},\mathbf{x}')\nabla' c(\mathbf{x}')] \cdot \hat{\mathbf{n}}(\mathbf{x}')dS' = \int_S [c(\mathbf{x}')\partial'_n G_0(\mathbf{x},\mathbf{x}') - G_0(\mathbf{x},\mathbf{x}')\partial'_n c(\mathbf{x}')]\, dS' \tag{27}$$

where $\hat{\mathbf{n}}$ is the outward normal to S and ∂'_n, as shown in Fig.1 denotes derivatives along $\hat{\mathbf{n}}$. Thus:

$$\int_V \left[c(\mathbf{x}')\nabla'^2 G_0(\mathbf{x},\mathbf{x}') - G_0(\mathbf{x},\mathbf{x}')\nabla'^2 c(\mathbf{x}')\right] dV' = \int_S [c(\mathbf{x}')\partial'_n G_0(\mathbf{x},\mathbf{x}') - G_0(\mathbf{x},\mathbf{x}')\partial'_n c(\mathbf{x}')]\, dS' \tag{28}$$

Since $G_0(\mathbf{x},\mathbf{x}') = -1/(4\pi D_v|\mathbf{x}-\mathbf{x}'|)$, the above integrals are singular for $\mathbf{x} = \mathbf{x}'$, and therefore we need to address the question of their existence. This translates into discussing separately the case where $\mathbf{x} \notin S$ and the case where $\mathbf{x} \in S$. In both cases the singularities have to be isolated in a subdomain of radius $\epsilon \to 0$ which is removed from the region of integration [2]. A rigorous derivation is provided in AppendixA.
In particular, if we define a function:

$$\omega(\mathbf{x}) = \begin{cases} \frac{1}{2} & \mathbf{x} \in S \\ 1 & \mathbf{x} \notin S,\ \mathbf{x} \in V \\ 0 & \mathbf{x} \notin V \end{cases} \tag{29}$$

Eq. (28) can be rewritten as:

$$-\int_V dV' G_0(\mathbf{x},\mathbf{x}')\rho(\mathbf{x}') + D_v \int_S dS' \left[c(\mathbf{x}')\partial'_n G_0(\mathbf{x},\mathbf{x}') - \partial'_n c(\mathbf{x}')G_0(\mathbf{x},\mathbf{x}')\right] = \omega(\mathbf{x})c(\mathbf{x}) \tag{30}$$

where $\rho(\mathbf{x}) = -D_v\nabla^2 c(\mathbf{x})$.
We now consider again our original problem and identify the region V as that occupied by the material, excluding the cavities, and $S = \left\{\cup_{i=1}^N \Sigma_i\right\} \cup S_e$. In this case $\rho(\mathbf{x})/\Omega$ is the number of vacancies generated at point $\mathbf{x}$ per unit time and unit volume. Since by its definition there are no sources of vacancies inside V, we can set $\rho(\mathbf{x}) = 0$. In addition:

$$D_v \partial'_n c(\mathbf{x})\Big|_{\mathbf{x}\in S} = -\Omega J_n(\mathbf{x})\Big|_{\mathbf{x}\in S}, \tag{31}$$

and therefore we can write the equation as follows:

$$\omega(\mathbf{x})c(\mathbf{x}) = \int_{S_e} dS' \left[D_v c(\mathbf{x}')\partial'_n + \Omega J_n(\mathbf{x})\right] G_0(\mathbf{x},\mathbf{x}') + \sum_{i=1}^{N} \int_{\Sigma_i} dS' \left[D_v c(\mathbf{x}')\partial'_n + \Omega J_n(\mathbf{x})\right] G_0(\mathbf{x},\mathbf{x}') \quad (32)$$

Eq. (32) is an *integral representation* of the solution inside the region V, however it does not provide a closed-form expression for the solution of the diffusion problem. In fact, it appears that $c(\mathbf{x})$ can be calculated in V only if $c(\mathbf{x})$ itself and its normal derivatives are known on the boundary surface S. In the following section we will define a self-consistent scheme to solve the problem.

2.3. Self-consistent solution

Consider a cavity exchanging vacancies with the material region and altering its shape as a consequence of the vacancy flow. In an infinitesimal time δt the surface area of the cavity changes by δA given by:

$$\delta A = 2\Omega\delta t \int_{\Sigma} dS\, \kappa(\mathbf{x}) J_n(\mathbf{x}) \quad (33)$$

where Σ represents the surface of the cavity, and $\kappa(\mathbf{x})$ is the local mean surface curvature, defined as:

$$\kappa(\mathbf{x}) = -\frac{1}{2}\nabla \cdot \hat{\mathbf{n}}(\mathbf{x}) \quad (34)$$

where $\hat{\mathbf{n}}(\mathbf{x})$ is the local normal vector to Σ, pointing in the outward direction with respect to V.
If we denote the vacancy concentration at $\mathbf{x} \in \Sigma$ as $c_\Sigma(\mathbf{x})$, then the local vacancy chemical potential at $\mathbf{x}$ is:

$$\mu_{\mathrm{v}}(\mathbf{x}) = k_B T \ln \frac{c_\Sigma(\mathbf{x})}{c_0} \quad (35)$$

The change in free energy related to vacancy exchange between bulk and cavity is therefore given by:

$$\delta F = \delta t \int_{\Sigma} dS \left[2\Omega\gamma\kappa(\mathbf{x}) - k_B T \ln \frac{c_\Sigma(\mathbf{x})}{c_0}\right] J_n(\mathbf{x}) \quad (36)$$

where γ is the cavity surface energy per unit area. By imposing again local thermodynamic equilibrium, i.e.:

$$2\Omega\gamma\kappa(\mathbf{x}) - k_B T \ln \frac{c_\Sigma(\mathbf{x})}{c_0} = 0 \quad (37)$$

we obtain an analogue of eq.19:

$$c_\Sigma(\mathbf{x}) = c_0 \exp\left[\frac{2\Omega\gamma\kappa(\mathbf{x})}{k_B T}\right] \quad (38)$$

The same result can be obtained in the case of the external surface S_e, following an identical derivation. The unknown normal fluxes can be more conveniently expressed as:

$$\begin{aligned} \Omega J_n(\mathbf{x})\Big|_{\mathbf{x}\in\Sigma_i} &= v_{\Sigma_i}(\mathbf{x}) \\ \Omega J_n(\mathbf{x})\Big|_{\mathbf{x}\in S_e} &= -v_{S_e}(\mathbf{x}) \end{aligned} \quad (39)$$

where $v_{\Sigma_i}(\mathbf{x})$ and $v_{S_e}(\mathbf{x})$ are the normal velocities of a point belonging to the i-th cavity or to the external surface, respectively, which are related to the total rate of change of the volume occupied by the medium as:

$$\frac{dV}{dt} = \frac{dV_{S_e}}{dt} - \sum_{i=1}^{N} \frac{dV_{\Sigma_i}}{dt} = \int_{S_e} v_{S_e}(\mathbf{x}) dS - \sum_{i=1}^{N} \int_{\Sigma_i} v_{\Sigma_i}(\mathbf{x}) dS \quad (40)$$

In summary, we can express the vacancy concentration inside the material region as a sum of surface

integrals:

$$\omega(\mathbf{x})c(\mathbf{x}) = \sum_{i=1}^{N} I_{\Sigma_i}(\mathbf{x}) + I_{S_e}(\mathbf{x}) \tag{41}$$

where:

$$\begin{aligned} I_{\Sigma_i}(\mathbf{x}) &= \int_{\Sigma_i} dS' \left[D_v c_s^i \partial'_n G_0(\mathbf{x}, \mathbf{x}') + v_{\Sigma_i}(\mathbf{x}) G_0(\mathbf{x}, \mathbf{x}') \right] \\ I_{S_e}(\mathbf{x}) &= \int_{S_e} dS' \left[D_v c_{S_e} \partial'_n G_0(\mathbf{x}, \mathbf{x}') - v_{S_e}(\mathbf{x}) G_0(\mathbf{x}, \mathbf{x}') \right] \end{aligned} \tag{42}$$

or, by writing each term explicitly:

$$\begin{aligned} I_{\Sigma_i}(\mathbf{x}) &= -\frac{1}{4\pi} \int_{\Sigma_i} dS' \left\{ \frac{\hat{\mathbf{n}}(\mathbf{x}') \cdot (\mathbf{x} - \mathbf{x}')}{|\mathbf{x} - \mathbf{x}'|^3} \exp\left[-\frac{\Omega\gamma \nabla \cdot \hat{\mathbf{n}}(\mathbf{x}') + E_v}{k_B T} \right] + \frac{v_{\Sigma_i}(\mathbf{x}')}{D_v |\mathbf{x} - \mathbf{x}'|} \right\} \\ I_{S_e}(\mathbf{x}) &= -\frac{1}{4\pi} \int_{S_e} dS' \left\{ \frac{\hat{\mathbf{n}}(\mathbf{x}') \cdot (\mathbf{x} - \mathbf{x}')}{|\mathbf{x} - \mathbf{x}'|^3} \exp\left[-\frac{\Omega\gamma \nabla \cdot \hat{\mathbf{n}}(\mathbf{x}') + E_v}{k_B T} \right] - \frac{v_{S_e}(\mathbf{x}')}{D_v |\mathbf{x} - \mathbf{x}'|} \right\} \end{aligned} \tag{43}$$

The above integrals can be evaluated, in general, by discretizing the surfaces of integration into triangular meshes, in a technique known as the *Boundary Element Method* (BEM) [2]. In the following sections we will show how, under certain assumptions, it is possible to obtain closed-form expressions for the surface velocities, without the need to employ a discretization scheme.

3. Spherical cavities and circular prismatic loops in the dilute limit

Consider the problem of N spherical cavities with surfaces $\Sigma_{i=1,...,N}$, embedded in a spherical medium of external surface S_e. We restrict ourselves to the case where the distances between individual objects are much greater than their sizes (*dilute limit*). In doing so, we are allowed to neglect the effect of the elastic field generated by dislocation loops on the local vacancy concentrations in the neighbourhood of the other objects, and, letting $\mathbf{x} \in \Sigma_k$, we can also use the approximation:

$$\sum_{i=1}^{N} I_{\Sigma_i}(\mathbf{x}) + I_{S_e}(\mathbf{x}) \approx \sum_{i \neq k} I_{\Sigma_i}(\bar{\mathbf{x}}_{\Sigma_k}) + I_{S_e}(\bar{\mathbf{x}}_{\Sigma_k}) + I_{\Sigma_k}(\mathbf{x}) \tag{44}$$

where $\bar{\mathbf{x}}_{\Sigma_k}$ denotes the geometrical centre of cavity Σ_k.
In addition, since each surface has spherical symmetry, we have:

$$c(\mathbf{x} \in \Sigma_k) = c_{\Sigma_k} \qquad \forall \mathbf{x} \in \Sigma_k, \, \forall \, k = 1, ..., N \tag{45}$$

and in the same way, using the assumption of diluteness, we can approximate:

$$v_{\Sigma_k}(\mathbf{x}) \approx v_{\Sigma_k} \qquad \forall \mathbf{x} \in \Sigma_k, \, \forall \, k = 1, ...N \tag{46}$$

If the distribution of objects inside the spherical medium is effectively homogeneous, we can similarly consider c_{S_e} and v_{S_e} to be constant on S_e. Under the previous assumptions, it is possible to evaluate analytically the surface integrals, without the need to use a discretization scheme.
We start by considering I_{Σ_i}. We separate two cases:

1. The field point $\mathbf{x}$ is on Σ_i
2. The field point $\mathbf{x}$ is not on Σ_i

In the following we will refer to the first case as the *self-interaction* contribution and to the latter as the *far-field* contribution. We adopt spherical coordinates with origin in the centre of the i-th cavity, i.e.:

$$\begin{cases} x = r \cos\phi \sin\theta \\ y = r \sin\phi \sin\theta \\ z = r \cos\theta \end{cases} \tag{47}$$

$$\begin{cases} x' = r'\cos\phi'\sin\theta' \\ y' = r'\sin\phi'\sin\theta' \\ z' = r'\cos\theta' \end{cases} \tag{48}$$

Since they are performed on spherical surfaces of constant radius r', the integrals have to be independent of θ and ϕ. Therefore we just need:

$$\begin{aligned} G_0(\mathbf{x},\mathbf{x}')\Big|_{\theta,\phi=0} &= -\frac{1}{4\pi D_v}\frac{1}{\sqrt{r^2+r'^2-2rr'\cos\theta'}} \\ \partial'_n G_0(\mathbf{x},\mathbf{x}')\Big|_{\theta,\phi=0} &= -\frac{\partial}{\partial r'}G_0(\mathbf{x},\mathbf{x}')\Big|_{\theta,\phi=0} = -\frac{1}{4\pi D_v}\frac{r'-r\cos\theta'}{\left(r^2+r'^2-2rr'\cos\theta'\right)^{3/2}} \end{aligned} \tag{49}$$

Let $a(t)$ be the radius of the cavity at time t, from which: $v_\Sigma = da/dt$.
For the self-interaction contribution we have $r = r' = a$, so that

$$\begin{aligned} I_\Sigma^{\text{self}} &= -\frac{1}{2D_v}\int_0^\pi \left[D_v c_\Sigma \frac{1-\cos\theta'}{2\sqrt{2}\left(1-\cos\theta'\right)^{3/2}} + \frac{da}{dt}\frac{a}{\sqrt{2}\sqrt{1-\cos\theta'}}\right]\sin\theta' d\theta' = \\ &= -\frac{1}{2\sqrt{2}}\left(\frac{c_\Sigma}{2}+\frac{a}{D_v}\frac{da}{dt}\right)\int_0^\pi \frac{\sin\theta'}{\sqrt{1-\cos\theta'}}d\theta' = -\frac{c_\Sigma}{2}-\frac{a}{D_v}\frac{da}{dt} \end{aligned} \tag{50}$$

while for the far-field case we have to compute:

$$I_\Sigma^{\text{far}} = -\frac{a^2}{2D_v}\int_0^\pi \sin\theta'\left[D_v c_\Sigma \frac{a-r\cos\theta'}{\left(r^2+a^2-2ar\cos\theta'\right)^{3/2}} + \frac{da}{dt}\frac{1}{\sqrt{r^2+a^2-2ar\cos\theta'}}\right]d\theta' = -\frac{a^2}{D_v r}\frac{da}{dt} \tag{51}$$

In summary:

$$I_\Sigma = \begin{cases} -\frac{c_\Sigma}{2}-\frac{a}{D_v}\frac{da}{dt} & |\mathbf{x}-\mathbf{x_0}| = a \\ -\frac{a^2}{D_v|\mathbf{x}-\mathbf{x_0}|}\frac{da}{dt} & |\mathbf{x}-\mathbf{x_0}| > a \end{cases} \tag{52}$$

where x_0 denotes the centre of the cavity under consideration.
Now consider I_{S_e} and let R_{out} be the radius of S_e. The self-interaction contribution can be computed in a matter analogous to the previous case:

$$\begin{aligned} I_{S_e}^{\text{self}} &= \frac{1}{2D_v}\int_0^\pi \left[D_v c_{S_e}\frac{1-\cos\theta'}{2\sqrt{2}\left(1-\cos\theta'\right)^{3/2}} + \frac{v_{S_e}R_{\text{out}}}{\sqrt{2}\sqrt{1-\cos\theta'}}\right]\sin\theta' d\theta' = \\ &= \frac{1}{2\sqrt{2}}\left(\frac{c_{S_e}}{2}+\frac{v_{S_e}R_{\text{out}}}{D_v}\right)\int_0^\pi \frac{\sin\theta'}{\sqrt{1-\cos\theta'}}d\theta' = \frac{c_{S_e}}{2}+\frac{v_{S_e}R_{\text{out}}}{D_v} \end{aligned} \tag{53}$$

where R_{out} is the radius of the external surface and $c_{S_e} = c(|\mathbf{x}| = R_{\text{out}})$. On the other hand:

$$\begin{aligned} I_{S_e}^{\text{far}} &= \frac{R_{\text{out}}^2}{2D_v}\int_0^\pi \sin\theta'\left[D_v c_{S_e}\frac{R_{\text{out}}-r\cos\theta'}{\left(r^2+R_{\text{out}}^2-2R_{\text{out}}r\cos\theta'\right)^{3/2}} + \frac{v_{S_e}}{\sqrt{r^2+R_{\text{out}}^2-2R_{\text{out}}r\cos\theta'}}\right]d\theta' = \\ &= c_{S_e}+\frac{v_{S_e}R_{\text{out}}}{D_v} \end{aligned} \tag{54}$$

3.1. Prismatic dislocation loops as toroidal sinks

In the treatment of Gu et al. [1] dislocations lines are modelled as 1D sinks. An alternative, which is more consistent with our treatment of cavities, is to consider them as tubes of radius r_d acting as surface sinks. In the first case, the expression for the vacancy concentration has to be supplemented by the term:

$$-\int_V dV' G_0(\mathbf{x}',\mathbf{x})\rho(\mathbf{x}') = \int_V dV' G_0(\mathbf{x}',\mathbf{x})b_e(\mathbf{x}')v_{\text{cl}}(\mathbf{x}')\delta\left(\Gamma\right) = \int_\Gamma dl' G_0(\mathbf{x}',\mathbf{x})b_e(\mathbf{x}')v_{\text{cl}}(\mathbf{x}') \tag{55}$$

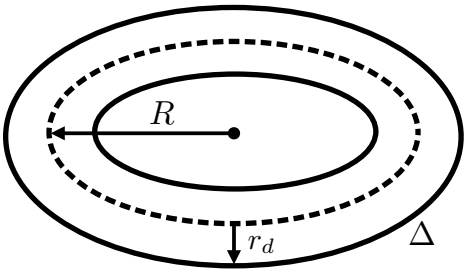

Figure 2: Schematic diagram of the torus defined by a circular dislocation loop.

arising from the first integral of eq.30. In particular, for a circular prismatic dislocation loop, i.e. $b_e(\mathbf{x}) = b$, assuming the dislocation core r_d to be much smaller than the loop radius R, we have [1]:

$$\int_\Gamma dl' G_0(\mathbf{x}', \mathbf{x}) b_e(\mathbf{x}') v_{\rm cl}(\mathbf{x}') \approx \begin{cases} -\frac{b \ln(8R/rd)}{2\pi D_v} v_{\rm cl} & \mathbf{x} \in \Gamma \\ \\ -\frac{bR}{2D_v |\mathbf{x}-\mathbf{x_0}|} v_{\rm cl} & |\mathbf{x} - \mathbf{x_0}| \gg R \end{cases} \tag{56}$$

where $\mathbf{x_0}$ is the position of the centre of the loop. We assumed that the defect separation is sufficiently large in order for $v_{\rm cl}$ to be roughly constant on the loop. We also neglected the effects of the elastic field generated by the loop on the structure of the diffusion Green's function, which in general will depend on the local hydrostatic pressure.
If we model the dislocation loop as a toroidal surface, on the other hand, we have to add additional terms of the form:

$$I_{\Delta_i} = D_v \int_{\Delta_i} dS' \left[c(\mathbf{x}') \partial'_n G_0(\mathbf{x}, \mathbf{x}') - \partial'_n c(\mathbf{x}') G_0(\mathbf{x}, \mathbf{x}') \right] \tag{57}$$

where Δ_i denotes the surface of the i-th dislocation tube. We prove that, under the dilute limit, the two treatments are equivalent.
Consider a toroidal dislocation tube, which surface we denote by Δ, with a revolution radius R (the radius of the dislocation loop) and a tube radius r_d, as shown in Fig.2.

We can straightforwardly evaluate the normal derivative of the vacancy concentration on the tube as:

$$\partial'_n c(\mathbf{x}') \Big|_{\mathbf{x}' \in \Delta} = -\frac{b v_{\rm cl}}{2\pi r_d D_v} \tag{58}$$

Furthermore, we can parametrise each point $\mathbf{x}' \in \Delta$ as:

$$\begin{cases} x' &= (R + r_d \cos\theta') \cos\phi' \\ y' &= (R + r_d \cos\theta') \sin\phi' \\ z' &= r_d \sin\theta' \end{cases} \tag{59}$$

where $\theta', \phi' \in [0, 2\pi)$. The surface element on the torus is then given by:

$$dS' = r_d (R + r_d \cos\phi') d\theta' d\phi' \tag{60}$$

and the inward normal to the surface is:

$$\hat{\mathbf{n}} = -\left(\cos\theta' \cos\phi', \cos\theta' \sin\phi', \sin\theta'\right) \tag{61}$$

from which it follows:

$$\partial'_n G_0(\mathbf{x}, \mathbf{x}') = \nabla' G_0(\mathbf{x}, \mathbf{x}') \cdot \hat{\mathbf{n}} = \frac{(x - x')\cos\theta' \cos\phi' + (y - y')\cos\theta' \sin\phi' + (z - z')\sin\theta'}{4\pi D_v |\mathbf{x} - \mathbf{x}'|^3} \tag{62}$$

We start by considering the case where $|\mathbf{x} - \mathbf{x}'| \gg R$, allowing us to approximate $|\mathbf{x} - \mathbf{x}'| \approx |\mathbf{x} - \mathbf{x_0}|$.

We also define $c_\Delta = c(\mathbf{x} \in \Delta)$. We obtain:

$$I_\Delta \approx D_v \int_0^{2\pi} d\theta' \int_0^{2\pi} d\phi' r_d (R + r_d \cos\phi') \left[c_\Delta \frac{(x-x_0)\cos\theta'\cos\phi' + (y-y_0)\cos\theta'\sin\phi' + (z-z_0)\sin\theta'}{4\pi D_v |\mathbf{x}-\mathbf{x_0}|^3} + \right.$$
$$\left. - \frac{b v_{\mathrm{cl}}}{2\pi r_d D_v} \frac{1}{4\pi D_v |\mathbf{x}-\mathbf{x_0}|} \right] = -\frac{bR}{2D_v|\mathbf{x}-\mathbf{x_0}|} v_{\mathrm{cl}} \tag{63}$$

which is the same far-field result obtained by considering the dislocation as a simple line source.
If $\mathbf{x} \in \Delta$, without loss of generalisation we can consider only the particular case for which the toroidal coordinate $\phi = 0$:

$$\begin{cases} x &= R + r_d \cos\theta \\ y &= 0 \\ z &= r_d \sin\theta \end{cases} \tag{64}$$

giving:

$$|\mathbf{x}-\mathbf{x}'|^2 = 2R^2 \left\{ (1-\cos\phi') \left[1 + \frac{r_d}{R} (\cos\theta + \cos\theta') \right] + O\left[\left(\frac{r_d}{R} \right)^2 \right] \right\} \tag{65}$$

and, neglecting second order contributions in r_d/R:

$$\begin{aligned} G_0(\mathbf{x},\mathbf{x}') &\approx \frac{1}{4\sqrt{2}\pi D_v R \sqrt{(1-\cos\phi')\left[1 + \frac{r_d}{R}(\cos\theta + \cos\theta')\right]}} \\ \partial'_n G_0(\mathbf{x},\mathbf{x}') &\approx \frac{(1-\cos\phi')\cos\theta' + \frac{r_d}{R}\left(\cos\theta\cos\theta'\cos\phi + \sin\theta\sin\theta' - 1\right)}{8\sqrt{2}\pi D_v R^2 \left\{(1-\cos\phi')\left[1 + \frac{r_d}{R}(\cos\theta+\cos\theta')\right]\right\}^{3/2}}. \end{aligned} \tag{66}$$

Therefore we obtain:

$$\begin{aligned} I^s_\Delta &= -D_v \int_\Delta dS' \partial'_n c(\mathbf{x}') G_0(\mathbf{x},\mathbf{x}') \approx \\ &\approx -\frac{b v_{\mathrm{cl}}}{8\sqrt{2}\pi^2 D_v} \int_0^{2\pi} d\phi' \int_0^{2\pi} d\theta' \frac{1 + \frac{r_d}{R}\cos\theta'}{\sqrt{(1-\cos\phi')\left[1 + \frac{r_d}{R}(\cos\theta+\cos\theta')\right]}} \end{aligned} \tag{67}$$

and:

$$\begin{aligned} I^d_\Delta &= D_v \int_{\Delta_i} dS' c(\mathbf{x}') \partial'_n G_0(\mathbf{x},\mathbf{x}') \approx \\ &\approx \frac{c_\Delta r_d}{8\sqrt{2}\pi R} \int_0^{2\pi} d\phi' \int_0^{2\pi} d\theta' \frac{(1-\cos\phi')\cos\theta' + \frac{r_d}{R}\left[\cos\theta'\cos\phi'(\cos\theta - \cos\theta') + \sin\theta'(\sin\theta + \sin\theta')\right]}{\left\{(1-\cos\phi')\left[1 + \frac{r_d}{R}(\cos\theta+\cos\theta')\right]\right\}^{3/2}} \end{aligned} \tag{68}$$

In order to simplify the notation, we define $\beta = r_d/R$ and:

$$\begin{aligned} J^s(\theta,\theta',\phi') &= \frac{1 + \beta\cos\theta'}{\sqrt{(1-\cos\phi')\left[1 + \beta(\cos\theta + \cos\theta')\right]}} \\ J^d(\theta,\theta',\phi') &= \frac{(1-\cos\phi')\cos\theta' + \beta\left[\cos\theta'\cos\phi'(\cos\theta - \cos\theta') + \sin\theta'(\sin\theta + \sin\theta')\right]}{\left\{(1-\cos\phi')\left[1 + \beta(\cos\theta+\cos\theta')\right]\right\}^{3/2}} \end{aligned} \tag{69}$$

We are concerned with the limiting case of $r_d \ll R$, i.e. $\beta \ll 1$, therefore we expand the above functions

to retain only fist order contributions in β:

$$J^s(\theta,\theta',\phi') \approx \frac{1+\frac{\beta}{2}(\cos\theta'-\cos\theta)}{\sqrt{1-\cos\phi}}$$
$$J^d(\theta,\theta',\phi') \approx \frac{\cos\theta'}{\sqrt{1-\cos\phi'}} + \beta\left[\frac{\cos\theta'\cos\phi'(\cos\theta-\cos\theta')+\sin\theta'(\sin\theta+\sin\theta')}{(1-\cos\phi')^{3/2}} - \frac{3\cos\theta'(\cos\theta+\cos\theta')}{2\sqrt{1-\cos\phi'}}\right] \tag{70}$$

Moreover, since we are treating $\partial'_n c_\Delta$ to be constant on Δ, we have to compute the averages of $J^s(\theta,\theta',\phi')$ and $J^d(\theta,\theta',\phi')$ with respect to θ. In particular we have, again to first order in β:

$$\bar{J}^s(\theta',\phi') = \frac{\int_0^{2\pi} J^s(\theta,\theta',\phi')d\theta}{2\pi} \approx \frac{1+\frac{\beta}{2}\cos\theta'}{\sqrt{1-\cos\phi'}}$$
$$\bar{J}^d(\theta',\phi') = \frac{\int_0^{2\pi} J^d(\theta,\theta',\phi')d\theta}{2\pi} \approx \frac{\cos\theta'}{\sqrt{1-\cos\phi'}} - \beta\left[\frac{3\cos^2\theta'}{2\sqrt{1-\cos\phi'}} + \frac{\cos^2\theta'\cos\phi'}{(1-\cos\phi)^{3/2}} - \frac{\sin^2\theta'}{(1-\cos\phi)^{3/2}}\right] \tag{71}$$

The integrations in θ' can be directly performed, giving:

$$\int_0^{2\pi} \bar{J}^s(\theta',\phi')d\theta' = \frac{2\pi}{\sqrt{1-\cos\phi'}}$$
$$\int_0^{2\pi} \bar{J}^d(\theta',\phi')d\theta' = -\frac{\pi\beta}{2\sqrt{1-\cos\phi'}} \tag{72}$$

on the other hand, both terms have non-integrable singularities for $\phi'=0$ and $\phi'=2\pi$. Even if we included the terms of order β^2 in Eq. (65), we would still retain the singular behaviour in the case of $\theta=\theta'$. In order to regularize the integrals, we perform the substitution:

$$|\mathbf{x}-\mathbf{x}'| \to \sqrt{|\mathbf{x}-\mathbf{x}'|+d_0^2}$$
$$\sqrt{1-\cos\phi'} \to \sqrt{1-\cos\phi'+\frac{d_0^2}{2R^2}} \tag{73}$$

where d_0 represents a small cut-off distance preventing self interaction. In particular:

$$\int_0^{2\pi} \frac{d\phi'}{\sqrt{1-\cos\phi'+\frac{d_0^2}{2R^2}}} = \frac{4}{\sqrt{2+\frac{d_0^2}{2R^2}}} K\left[\frac{2}{2+\frac{d_0^2}{2R^2}}\right] \approx 2\sqrt{2}\ln\left(\frac{8R}{d_0}\right) \tag{74}$$

where $K(m)=\int_0^{2\pi}(1-m\sin^2\theta)dx$ is the complete elliptic integral of the first kind. In summary we have that, to leading order in β:

$$I^s_\Delta \approx -\frac{b_e v_{\rm cl}}{2\pi D_v}\ln\left(\frac{8R}{d_0}\right)$$
$$I^d_\Delta \approx -\frac{\beta^2 c_\Delta}{8}\ln\left(\frac{8R}{d_0}\right) \tag{75}$$

the term I^d_Δ, being of order β^2, can be neglected, while I^s_Δ recovers the result in eq.56 if we identify the cut-off radius d_0 with r_d.
The self climb force acting on a prismatic dislocation loop can also be analytically calculated, and in the elastically-isotropic case is given by [23]:

$$f_{\rm cl} = \pm\frac{\mu b^2}{4\pi(1-\nu)R}\left[\ln\left(\frac{8R}{r_d}\right)-1\right] \tag{76}$$

where the plus and minus signs represent respectively the case of an interstitial or vacancy loop, μ is the shear modulus and ν is Poisson's ratio. In the dilute limit elastic interactions between different loops are much smaller than self-interactions, and therefore we neglect them in the present treatment.

3.2. Matrix formulation in the dilute limit

We consider a general dilute configuration with M circular prismatic dislocations loops, of radii $\{R_k\}_{k=1}^{M}$, and N spherical cavities, of radii $\{R_j\}_{j=M+1}^{M+N}$, embedded in a spherical medium of radius R_{out}.
We can write a set of N+M equations of the form:

$$c_i = \sum_{k=1}^{M} I_{\Delta_k}(\mathbf{x}_i) + \sum_{j=1}^{N} I_{\Sigma_j}(\mathbf{x}_i) + I_{S_e}(\mathbf{x}_i) \qquad i = 1, .., N+M \tag{77}$$

where c_i denotes the local vacancy concentration on the surface of the i-th object and $\mathbf{x}_i$ is the position of its centre.
We still need an additional equation in order to have a determined system for the $N+M+1$ unknowns, namely the $N+M$ growth rates dR_i/dt plus dR_{out}/dt.
Following from the assumption of a homogeneous distribution of defects inside the medium, we take the average of each surface integral with respect to a field point constrained on the sphere and we relate it to the vacancy concentration at the external surface:

$$c_{S_e} = \sum_{k=1}^{M} \langle I_{\Delta_k}(\mathbf{x}) \rangle_{\mathbf{x}\in S_e} + \sum_{j=1}^{N} \langle I_{\Sigma_j}(\mathbf{x}) \rangle_{\mathbf{x}\in S_e} + \langle I_{S_e}(\mathbf{x}) \rangle_{\mathbf{x}\in S_e} \tag{78}$$

which means that we need to compute:

$$\left\langle \frac{1}{|\mathbf{x}-\mathbf{x_0}|} \right\rangle_{\mathbf{x}\in S_e} = \frac{1}{4\pi R_{\text{out}}^2} 2\pi R_{\text{out}}^2 \int_0^{\pi} d\theta \frac{\sin\theta}{\sqrt{R_{\text{out}}^2 + r_0^2 - 2r_0 R_{\text{out}} \cos\theta}} = \frac{1}{R_{\text{out}}} \tag{79}$$

The complete set of equations is therefore given by:

$$\begin{aligned}
D_v\left(c_{S_e} - c_{\Sigma_i}\right) &= \sum_{k=1}^{M} \frac{bR_k\zeta_k}{|\mathbf{x}_i - \mathbf{x}_k|} \frac{dR_k}{dt} + \sum_{j=M+1,\, j\neq i}^{M+N} \frac{R_j^2}{|\mathbf{x}_i - \mathbf{x}_j|} \frac{dR_j}{dt} + R_i \frac{dR_i}{dt} - v_{S_e} R_{\text{out}} \\
D_v\left(c_{S_e} - c_{\Delta_i}\right) &= \sum_{k=1,\, k\neq i}^{M} \frac{bR_k\zeta_k}{|\mathbf{x}_i - \mathbf{x}_k|} \frac{dR_k}{dt} + \sum_{j=M+1}^{M+N} \frac{R_j^2}{|\mathbf{x}_i - \mathbf{x}_j|} \frac{dR_j}{dt} + \frac{b\ln(8R_i/r_d)}{2\pi} \frac{dR_i}{dt} - v_{S_e} R_{\text{out}} \\
0 &= \sum_{k=1}^{M} \frac{bR_k\zeta_k}{R_{\text{out}}} \frac{dR_k}{dt} + \sum_{j=M+1}^{M+N} \frac{R_j^2}{R_{\text{out}}} \frac{dR_j}{dt} - v_{S_e} R_{\text{out}}
\end{aligned} \tag{80}$$

where the factor ζ_i discriminates between vacancy and interstitial loops as:

$$\zeta_i = \begin{cases} +1 & \text{object } i \text{ is a vacancy loop} \\ -1 & \text{object } i \text{ is an interstitial loop} \end{cases} \tag{81}$$

By defining the dimensionless vectors $\boldsymbol{\nu}$:

$$\boldsymbol{\nu} = \frac{b}{D_v} \Bigg(\underbrace{\zeta_1 \frac{dR_1}{dt}, ..., \zeta_M \frac{dR_M}{dt}}_{\text{loops}}, \underbrace{\frac{R_{M+1}}{b}\frac{dR_{M+1}}{dt}, ..., \frac{R_{M+N}}{b}\frac{dR_{M+N}}{dt}}_{\text{cavities}}, \underbrace{\frac{v_{S_e} R_{\text{out}}}{b}}_{\text{outer surface}} \Bigg)^T \tag{82}$$

and $\tilde{\mathbf{c}}$:

$$\tilde{\mathbf{c}} = \left(c_{S_e} - c_{\Delta_1}, ..., c_{S_e} - c_{\Delta_M}, c_{S_e} - c_{\Sigma_1}, ..., c_{S_e} - c_{\Sigma_N}, 0 \right)^T \tag{83}$$

We can express the problem in matrix form as:

$$\mathbf{M} \cdot \boldsymbol{\nu} = \tilde{\mathbf{c}} \tag{84}$$

Where $\mathbf{M}$ is a $(M+N+1) \times (M+N+1)$ matrix given by:

$$\begin{bmatrix}
\frac{\ln(8R_1/r_d)}{2\pi} & \eta_{1,2} & \cdots & \cdots & \cdots & \cdots & \cdots & \eta_{1,M+N} & -1 \\
\eta_{2,1} & \ddots & \eta_{2,3} & \cdots & \cdots & \cdots & \cdots & \eta_{2,M+N} & -1 \\
\vdots & \vdots & \ddots & \vdots & \vdots & \vdots & \vdots & \vdots & \vdots \\
\eta_{M,1} & \cdots & \eta_{M,M-1} & \frac{\ln(8R_M/r_d)}{2\pi} & \eta_{M,M+1} & \cdots & \cdots & \eta_{M,M+N} & -1 \\
\eta_{M+1,1} & \cdots & \cdots & \eta_{M+1,M} & 1 & \eta_{M+1,M+2} & \cdots & \eta_{M+1,M+N} & -1 \\
\eta_{M+2,1} & \cdots & \cdots & \cdots & \eta_{M+2,M+1} & 1 & \cdots & \eta_{M+2,M+N} & -1 \\
\vdots & \vdots & \vdots & \vdots & \vdots & \vdots & \ddots & \vdots & \vdots \\
\eta_{M+N,1} & \cdots & \cdots & \cdots & \cdots & \cdots & \eta_{M+N,M+N-1} & 1 & -1 \\
\frac{R_1}{R_{\text{out}}} & \frac{R_2}{R_{\text{out}}} & \cdots & \frac{R_M}{R_{\text{out}}} & \frac{R_{M+1}}{R_{\text{out}}} & \cdots & \cdots & \frac{R_{M+N}}{R_{\text{out}}} & -1
\end{bmatrix}$$

and $\eta_{i,j} = \frac{R_j}{|\mathbf{x}_i - \mathbf{x}_j|}$.
Explicitly:

$$M_{ij} = \begin{cases}
\frac{R_j}{|\mathbf{x}_i - \mathbf{x}_j|} & i \neq j;\ i,j \neq M+N+1 \\
\frac{R_j}{R_{\text{out}}} & i \neq j;\ i = M+N+1 \\
-1 & j = M+N+1 \\
\frac{\ln(8R_i/r_d)}{2\pi} & i = j;\ i,j \leq M \\
1 & i = j;\ M < i,j < M+N+1
\end{cases} \tag{85}$$

Therefore, once the vacancy concentration is prescribed at the dislocation cores, at the surface of the cavities and at the external free surface, the rates of growth can be readily calculated as:

$$\boldsymbol{\nu} = \mathbf{M}^{-1} \tilde{\mathbf{c}} \tag{86}$$

where, under the local equilibrium assumption, we have:

$$\begin{aligned}
c_{\Delta_i} &= c_0 \exp\left(-\frac{f^i_{\text{cl}} \Omega}{b k_B T}\right) \\
c_{\Sigma_i} &= c_0 \exp\left(\frac{2\gamma\Omega}{R_{i+M} k_B T}\right) \\
c_{S_e} &= c_0 \exp\left(\frac{2\gamma\Omega}{R_{\text{out}} k_B T}\right)
\end{aligned} \tag{87}$$

where f^i_{cl} is the climb force acting on the i-th loop.
We remark that the above boundary conditions are derived from the free energy of defect clusters, calculated using linear elasticity and orientation-averaged surface energies, respectively for dislocation loops and cavities. We compared the cluster formation energies computed with such continuum methods and those obtained using atomistic calculations in W [24]. As shown in Fig.6 there is remarkable quantitative agreement between the continuum and atomistic treatment. It is clear at this point that

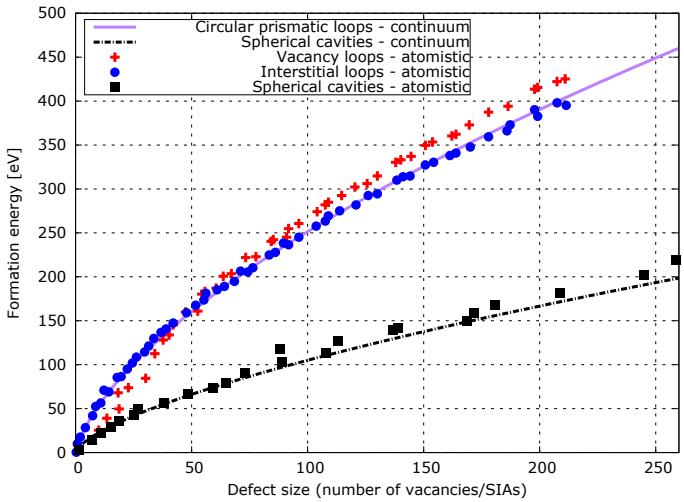

Figure 3: Relaxed formation energies of spherical cavities and $\frac{1}{2}\langle 111\rangle$ prismatic dislocation loops in W. Continuum expressions for the elastic energies of loops and the total surface energy of cavities are compared with atomistic energies calculated in [24] using many-body interatomic potentials.

our modelling implies an asymmetry in the dynamics of interstitials and vacancy loops, due to the fact that only vacancies are considered as diffusing point defects. In particular, consider an isolated circular prismatic loop in a infinite medium without supersaturation. The radius R of the loop changes in time as:

$$\frac{dR}{dt} = \zeta \frac{2\pi c_0 D_v}{b \ln \frac{8R}{r_d}} \left\{ 1 - \exp\left[\frac{\zeta \Omega |f_{\rm cl}|}{b k_B T} \right] \right\} \tag{88}$$

In the limit of $|f_{\rm cl}| \ll bk_BT/\Omega$ the above expression can be linearized, leading to:

$$\frac{dR}{dt} \approx \zeta^2 \frac{2\pi c_0 \Omega D_v}{b^2 k_B T \ln \frac{8R}{r_d}} |f_{\rm cl}| = \frac{2\pi c_0 \Omega D_v}{b^2 k_B T \ln \frac{8R}{r_d}} |f_{\rm cl}| \tag{89}$$

which does not depend on ζ, the loop type. However, in many realistic situations, such as in the case of small loops a few nanometers wide, the previous approximation cannot be justified. The full exponential relationship leads therefore to non-symmetric dynamics for large climb forces. In particular, vacancy loops will shrink faster than interstitial loops of the same size.
We also point out that the expressions in eq.87 are derived under the assumption of $c \ll 1$. In general, the correct expression for the vacancy concentration under a generalised thermodynamic driving force $\Phi(\mathbf{x})$ has the form of a generalised Fermi-Dirac distribution [25]:

$$c(\mathbf{x}) = \frac{c_0 \exp\left(-\frac{\Phi(\mathbf{x})}{k_B T}\right)}{1 + c_0 \left[\exp\left(-\frac{\Phi(\mathbf{x})}{k_B T}\right) - 1\right]} \tag{90}$$

which ensures $c < 1$. However, even in the extreme case of a prismatic vacancy loop with the smallest possible radius of the order of one Burgers vector, we have $c_\Delta \simeq 10^{-6}$ at $T = 2000$ K. For this reason the expressions of Eq. (87) can be safely used.

3.3. Simple configurations of cavities

In this section we will present some results obtained for simple configurations of cavities, in order to outline some basic features of the model.

3.3.1. Single cavity in an infinite medium

Consider a single cavity of radius R in an infinite medium with a bulk vacancy concentration of c_∞. This is equivalent to having an infinitely distant, static, outer surface with assigned concentration c_∞,

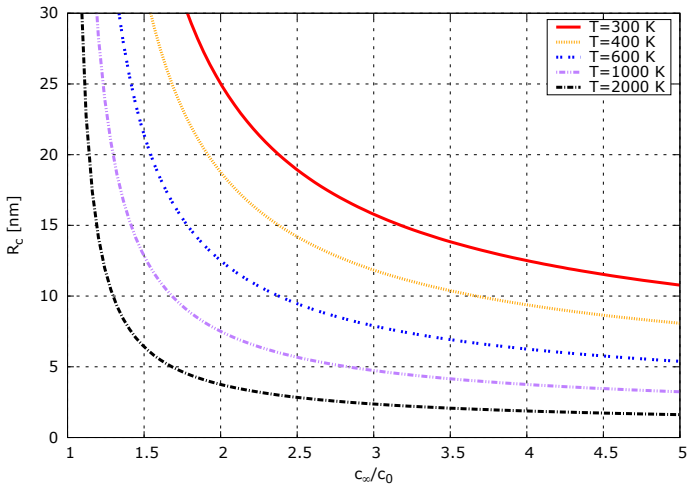

Figure 4: Critical cavity growth radius R_c in tungsten as a function of vacancy supersaturation ratio c_∞/c_0, for several temperatures in the range 300-2000 K. The relevant parameters used are: $\gamma = 20.38$ eV nm^{-2} and $\Omega = 0.011$ nm^3.

described by the matrix equation:

$$\frac{1}{D_v} \lim_{R_{\text{out}} \to \infty} \begin{pmatrix} 1 & -1 \\ \frac{R}{R_{\text{out}}} & -1 \end{pmatrix} \begin{pmatrix} R\frac{dR}{dt} \\ v_{S_e} R_{\text{out}} \end{pmatrix} = \begin{pmatrix} c_\infty - c_\Sigma \\ 0 \end{pmatrix} \tag{91}$$

leading to:

$$\begin{aligned} \lim_{R\text{out} \to \infty} R_{\text{out}} \frac{dR_{\text{out}}}{dt} &= 0 \\ \frac{dR}{dt} &= \frac{D_v c_0}{R} \left[\frac{c_\infty}{c_0} - \exp\left(\frac{2\gamma\Omega}{R_i k_B T} \right) \right] \end{aligned} \tag{92}$$

If there is no vacancy supersaturation in the medium, i.e. $c_\infty \leq c_0$, the cavity always shrinks in order to reduce its surface energy. However, if $c_\infty > c_0$, for certain values of R the cavity may grow in order to accommodate the free vacancies absorbed from the bulk.
We can define a critical radius R_c for which $dR/dt\big|_{R_c} = 0$, given by the equation:

$$R_c = \frac{2\gamma\Omega}{\log\left(\frac{c_\infty}{c_0}\right) k_B T} \tag{93}$$

and in particular we have:

$$\begin{cases} \frac{dR}{dT} < 0 & R < R_c \\ \frac{dR}{dT} > 0 & R > R_c \end{cases} \tag{94}$$

Several values of R_c as a function of temperature T and supersaturation ratio $\frac{c_\infty}{c_0}$ are shown in Fig.4, using the values of parameters $\gamma = 20.38$ eV nm^{-2} and $\Omega = 0.011$ nm^3.

3.3.2. Two cavities in an infinite medium

Consider two cavities of initial radii R_1 and R_2, the centres of which are separated by a distance r, embedded in an infinite medium with a bulk vacancy concentration c_∞. The growth rates of the two

cavities are governed by the matrix equation:

$$\frac{1}{D_v}\lim_{R\text{out}\to\infty}\begin{pmatrix}1 & \frac{R_2}{r} & -1\\ \frac{R_1}{r} & 1 & -1\\ \frac{R_1}{R_{\text{out}}} & \frac{R_2}{R_{\text{out}}} & -1\end{pmatrix}\begin{pmatrix}R_1\frac{dR_1}{dt}\\ R_2\frac{dR_2}{dt}\\ v_{S_e}R_{\text{out}}\end{pmatrix}=\begin{pmatrix}c_\infty-c_{\Sigma_1}\\ c_\infty-c_{\Sigma_2}\\ 0\end{pmatrix} \tag{95}$$

Solving for $v_{S_e}R_{\text{out}}$, and inverting the reduced 2×2 matrix we obtain:

$$\begin{pmatrix}R_1\frac{dR_1}{dt}\\ R_2\frac{dR_2}{dt}\end{pmatrix}=\frac{D_v}{1-\frac{R_1R_1}{r^2}}\begin{pmatrix}1 & -\frac{R_2}{r}\\ -\frac{R_1}{r} & 1\end{pmatrix}\begin{pmatrix}c_\infty-c_{\Sigma_1}\\ c_\infty-c_{\Sigma_2}\end{pmatrix} \tag{96}$$

Let $i,j=1,2$ and $i\neq j$, we have:

$$\begin{aligned}\frac{dR_i}{dt}&=\frac{D_v r}{(R_i r^2-R_i^2R_j)}\left[r\left(c_\infty-c_{\Sigma_i}\right)-R_j\left(c_\infty-c_{\Sigma_j}\right)\right]\\ &=\frac{1}{1-\frac{R_iR_j}{r^2}}\left[\left(\frac{dR_i}{dt}\right)_0-\frac{R_j^2}{rR_i}\left(\frac{dR_j}{dt}\right)_0\right]\end{aligned} \tag{97}$$

Here $\left(\frac{dR_k}{dt}\right)_0$ denotes the growth rate of cavity k in the non-interacting case.
In a particular case, where $R_1=R_2=R$, we have:

$$\frac{dR}{dt}=\frac{1}{1+\frac{R}{r}}\left(\frac{dR}{dt}\right)_0 \tag{98}$$

i.e. as the distance between the cavities decreases, the magnitude of $\left|\frac{dR}{dt}\right|$ also decreases. From a physical point of view the individual vacancy fluxes flowing to (or from) each cavity are reduced by the presence of a double sink.
In a general case of $R_1\neq R_2$, we have a more complex situation. Suppose that $R_2>R_1$; then the absolute value of dR_2/dt is monotonically increasing as a function of the inter-cavity distance d.

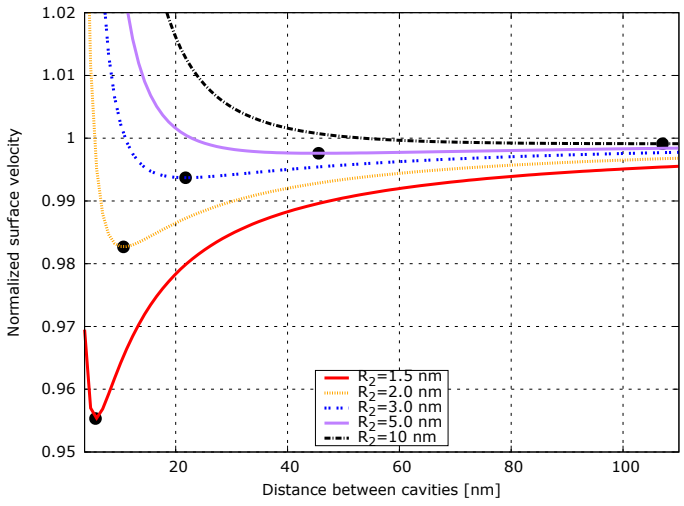

Figure 5: Surface velocity of 1 nm spherical cavity as a function of the distance from a second cavity of variable radius, normalized with respect to the case where there is no second cavity. The system is infinite and at a temperature of 1750 K, while the bulk vacancy concentration is set to its equilibrium value. Parameters of the model are chosen to describe tungsten. Black dots denote the minimum of normalized velocity.

On the other hand, we can define a critical value d_c:

$$d_c = \frac{R_1(c_\infty - c_{\Sigma_1})}{c_\infty - c_{\Sigma_2}} \left[1 + \sqrt{1 - \frac{R_2}{R_1} \left(\frac{c_\infty - c_{\Sigma_2}}{c_\infty - c_{\Sigma_1}} \right)^2} \right] \tag{99}$$

such that the absolute value $\frac{dR_2}{dt}$ increases with the inter-cavity distance for $d > d_c$ and decreases for $d < d_c$. In other terms, when the two cavities are sufficiently close, the larger one induces faster evaporation of the smaller one, in a process which is akin to the well-known Ostwald ripening.

3.4. Validation of the steady-state approximation

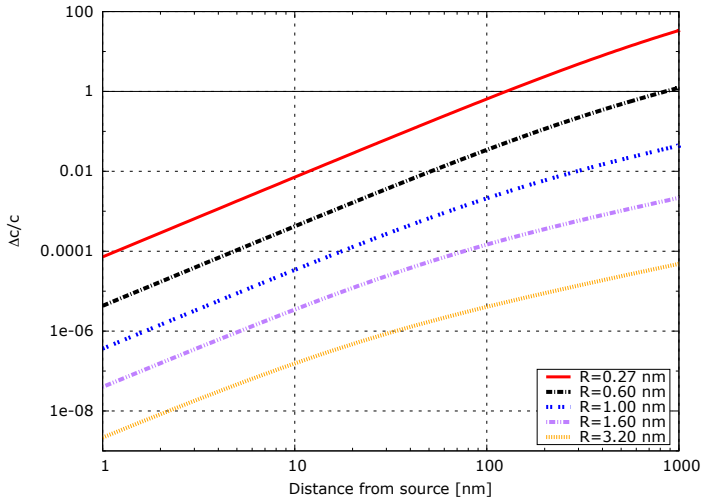

Figure 6: Relative variation $\Delta c/c$ of the vacancy field adiabatic with respect to a circular prismatic vacancy dislocation loop, as a function of the distance r from the vacancy loop, in W. The variation is calculated over a time $\tau(r) = \frac{r^2}{D_v}$, i.e. the approximate equilibration time of perturbations in the vacancy field. Several values of the dislocation loop radius are considered. The system temperature is 1750 K and $c_\infty = c_0$.

The method we described implicitly defines a steady-state concentration field $c(\mathbf{x}; t)$ which depends parametrically on time through $\Delta_i(t)$, $\Sigma_j(t)$ and $S_e(t)$. From a physical point of view this means that vacancy equilibration occurs on much shorter timescales than those related to the macroscopic evolution of defect clusters. We can now quantitatively validate this assumption *a posteriori*.
Consider a single circular prismatic vacancy loop of radius R inside an infinite medium with a bulk vacancy concentration c_∞. The steady-state, or *adiabatic*, vacancy concentration field $c(r; t)$ at time t and distance $r \gg R(t)$ from the centre of the loop is given by:

$$c(r; t) = c_\infty - \frac{bR(t)}{2D_v r}\dot{R}(t) = c_\infty - \frac{\pi R(t)}{r \ln \frac{8R(t)}{rd}}(c_\Delta(t) - c_\infty) \tag{100}$$

where $c_\Delta(t)$ is the vacancy concentration at the dislocation line, which also depends parametrically on time through $R(t)$. Therefore we can compute the rate of change of the adiabatic vacancy field as:

$$\frac{dc(r; t)}{dt} = \frac{\partial c(r; t)}{\partial R}\dot{R}(t) = \frac{2\pi^2 D_v (c_\Delta(t) - c_\infty)}{rb \ln \frac{8R(t)}{r_d}} \left[\frac{\Omega \mu b \, c_\Delta(t)}{4\pi(1-\nu)R(t)k_B T} - (c_\Delta(t) - c_\infty) \frac{\ln \frac{8R(t)}{r_d} - 1}{\left(\ln \frac{8R(t)}{r_d} \right)^2} \right] \tag{101}$$

On the other hand, the transient perturbation generated by the dislocation line motion propagates over a distance r in a time of the order of $\tau(r) \simeq r^2/D_v$. We can estimate the relative change in the adiabatic

vacancy concentration during a time $\tau(r)$ as:

$$\frac{\Delta c(r;t)}{c(r;t)} \simeq \frac{dc(r;t)}{dt}\frac{\tau(r)}{c(r;t)} \tag{102}$$

Eq.102 provides a quantitative measure that allows us to investigate the regime of applicability of the steady-state solution. In particular, solving the steady state problem as opposed to the full time-dependent one gives accurate results when $\Delta c(r;t)/c(r;t) \lesssim 1$, i.e. when the adiabatic field changes slowly with respect to the propagation of transient perturbations. In Fig.6 we plot the value $\Delta c/c$ as a function of r, for several values of the loop radius R, using material parameters for tungsten at a temperature of 1750 K and with $c_\infty = c_0$. We can see that for distances less than 100 nm from the loop, the condition of validity is respected even for the smallest possible loop size ($R = b = 0.27$ nm). At much larger distances of 1000 nm the condition is not respected for loops smaller than approximately 0.60 nm. We point out, however, that such small loops are typically present in the simulation cell for considerably shorter timescales than the bigger ones, since their climb velocities are exponentially greater. Interstitial loops and cavities evolve more slowly than vacancy loops, and in addition $\Delta c/c$ decreases at lower temperatures, therefore we conclude that the steady-state approximation adequately captures the cooperative evolution of defect clusters in systems of dimensions of the order of $100 - 1000$ nm.

3.5. Preliminary numerical results

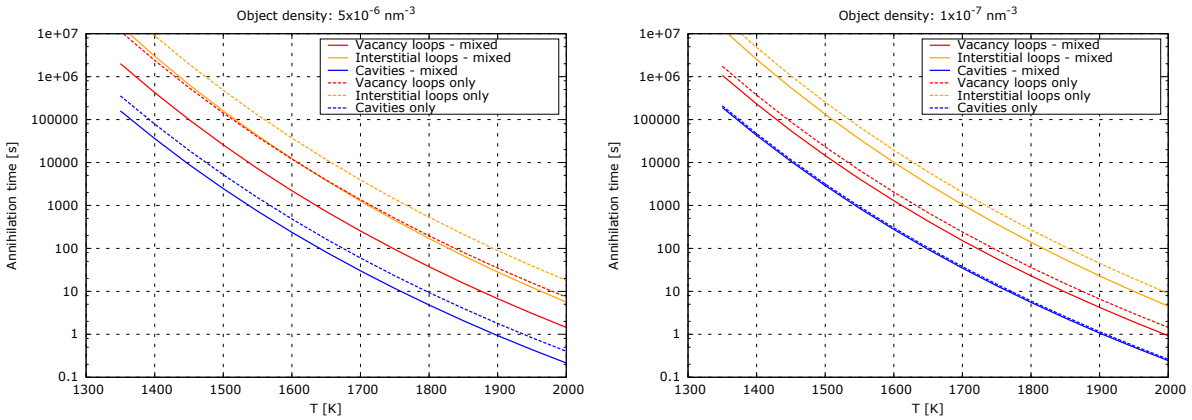

Figure 7: Total annihilation times in tungsten, as a function of annealing temperature for each object class: 1/2<111> prismatic vacancy loops (red lines) and interstitial loops (yellow lines), and spherical cavities (blue lines). Solid lines were obtained in the case 10 objects (30 in total) of each class in the simulation cell, while dashed lines were obtained in the case of 30 objects of the same class. a) The radius of the medium is 111.85 nm and the average object density is 5×10^{-6} nm^{-3}. b): The radius of the medium is 408.34 nm and the average object density is 1×10^{-7} nm^{-3}. The relevant simulation parameters are: shear modulus $\mu = 161$ Gpa, Poisson's ratio $\nu = 0.28$, Burgers vector $b = 0.274$ nm, dislocation core radius $r_d = 0.316$ nm, atomic volume $\Omega = 0.011$ nm^3, vacancy formation energy $E_v = 3.65$ eV and barrier for vacancy migration $E_{\text{mig}} = 1.78$ eV. The radii of the defects are normally distributed: with mean 3.2 nm and standard deviation 1 nm, in the case of dislocation loops, and with mean 1 nm and standard deviation 0.1 nm, in the case of cavities.

The model in the dilute limit has been implemented numerically in a `C++` code that, given an initial starting configuration of cavities and/or dislocation loops, solves the matrix equation determining individual growth rates, and performs time evolution of the object radii. As previously mentioned, long range elastic interactions between defects are neglected, and the climb force acting on dislocation loops is assumed to originate only from elastic self-interaction.
The physical parameters required as input are: surface energy density γ (eV/nm^2), shear modulus μ (GPa), Poisson's ratio ν, Burgers vector magnitude b (nm), dislocation core radius r_d (nm), atomic volume Ω (nm^3), vacancy formation energy E_v (eV), barrier for vacancy migration E_{mig} (eV), diffusion coefficient prefactor D_0 (nm^2/s), and annealing temperature T (K).

The integration time-step is dynamically updated in order to enforce the condition:

$$10^{-4} \leq \max_{1<i<N+M} \left\{ \frac{|\frac{dR_i}{dt}|}{R_i} \right\} \leq 10^{-3} \tag{103}$$

which has been found to give an adequate balance between numerical stability and computational times. Fig.7 shows data obtained using realistic parameters and object distributions, in the case of tungsten. A set of 10 vacancy dislocation loops, 10 interstitial loops and 10 cavities were randomly distributed inside a spherical medium. Object sizes were sampled from Gaussian distributions with mean 3.2 nm and standard deviation 1 nm, in the case of dislocation loops, and with mean 1 nm and standard deviation 0.1 nm, in the case of cavities. Such size distributions are consistent with the experimentally observable defects in neutron-irradiated tungsten [5, 3]. The same simulations were repeated in the case of 30 objects all of the same type in the simulation cell. In all cases we considered circular prismatic $\frac{1}{2}$<111> loops.

We have analysed two configurations: one having the defect density of 5×10^{-6} nm^{-3} and the system radius of 111.85 nm (Fig.7a), and the other having the defect density of 1×10^{-7} nm^{-3} and the system radius of 408.34 nm (Fig.7b). Simulations were performed in the temperature range between 1350 K and 2000 K. For each object class (i.e. vacancy loops, interstitial loops or cavities) we define an annihilation time as the time required for every object in the class to disappear. We can immediately note that the timescales depend exponentially on temperature, which is a feature typical for diffusion-driven dynamics. In particular, by fitting the annihilation time curves to the function:

$$f(T) = A \left[\exp\left(\frac{E}{k_B T} \right) - 1 \right] \tag{104}$$

we obtain the average value of parameter E equal to 5.2824 ± 0.0005 eV, which is remarkably close to the sum $E_v + E_{\text{mig}} = 5.34$ eV. More interestingly, the calculated annealing timescales are in quantitative agreement with experimental data of annealing of dislocation loops in W at ~ 1670 K [3].

When the simulation cell is populated by defect clusters of the same kind, increasing the cluster density produces longer annihilation timescales, which is particularly noticeable in the case of vacancy loops. As the distances between the defects are reduced, the local environment around each of them will present, on average, higher (in the case of vacancy loops and cavities) or lower (in the case of interstitial loops) vacancy concentrations with respect to the equilibrium value. It can also be noted that this effect is partially suppressed in the case where clusters of both interstitials and vacancy defects are present in the simulation cell.

This particular example highlights the fact that both defect density and defect distribution can influence the annealing timescales in a non-trivial way. In order to produce accurate quantitative estimates of annealing timescales, accurate knowledge on the relative abundance of various defect types is required. While it is straightforward to distinguish cavities from dislocation loops experimentally, it is much more difficult to characterize whether a given dislocation loop is of vacancy or interstitial type. This is especially true in the case of radiation-induced prismatic loops, which are only a few nanometers across. As a result, there is still no consensus yet on the relative abundance of vacancy and interstitial type prismatic loops in irradiated materials, particularly in the case of ion irradiated materials. In the case of W, some experiments report a roughly equal number of vacancy and interstitial $\frac{1}{2}$<111> loops [26], while others report a higher abundance of interstitial loops [27].

4. Conclusions

In this paper we derived an extension of the non-local model for dislocation climb of Gu et al. [1] to the case of a finite medium with cavities. We also presented a simplified formulation for the case of a dilute concentration of spherical cavities and circular prismatic loops. We have shown that the simplified model adequately predicts the timescales characterizing annealing of radiation defects in tungsten. The need for an accurate knowledge of the relative abundance of cluster types is highlighted to characterise precisely their annealing timescales.

Acknowledgements

IR and SLD were partly funded by the RCUK Energy Programme (grant No. EP/I501045). IR was also supported by the EPSRC Centre for Doctoral Training on Theory and Simulation of Materials at Imperial College London under grant number EP/L015579/1. This work was carried out within the framework of the EUROfusion Consortium and has received funding from the Euratom research and training programme 2014-2018 under grant agreement No. 633053. The views and opinions expressed herein do not necessarily reflect those of the European Commission. APS is grateful to the Blackett Laboratory for the provision of laboratory facilities.

AppendixA. Derivation of Kirchhoff integral representation

Here we present a rigorous derivation of eq.30, adapted from [2]. We start by considering the equation:

$$D_v \nabla^2 c(\mathbf{x}) = -\rho(x) \qquad \mathbf{x} \in V \tag{A.1}$$

AppendixA.1. Field point not belonging to S

Consider a fixed field point $\mathbf{x} \notin S$, and define V_ϵ as the ball of radius ϵ centred at $\mathbf{x}$, completely included in V, and let $\partial V_\epsilon = S_\epsilon$. By adapting Eq. (28) to the region $V - V_\epsilon$ and taking the limit as $\epsilon \to 0$, we have:

$$\begin{aligned}
&\lim_{\epsilon\to 0} \int_{V-V_\epsilon} c(\mathbf{x}')\nabla'^2 G_0(\mathbf{x},\mathbf{x}')dV' - \lim_{\epsilon\to 0} \int_{V-V_\epsilon} G_0(\mathbf{x},\mathbf{x}')\nabla'^2 c(\mathbf{x}')dV' = \\
&= \int_S \left[c(\mathbf{x}')\partial'_n G_0(\mathbf{x},\mathbf{x}') - G_0(\mathbf{x},\mathbf{x}')\partial'_n c(\mathbf{x}')\right] dS' + \lim_{\epsilon\to 0} \int_{S_\epsilon} \left[c(\mathbf{x}')\partial'_n G_0(\mathbf{x},\mathbf{x}') - G_0(\mathbf{x},\mathbf{x}')\partial'_n c(\mathbf{x}')\right] dS'
\end{aligned} \tag{A.2}$$

Since $D_v \nabla'^2 G_0(\mathbf{x},\mathbf{x}') = \delta(\mathbf{x}-\mathbf{x}')$ and by construction $\mathbf{x} \neq \mathbf{x}'$, the first term on the left hand side is identically zero.
We also have:

$$\lim_{\epsilon\to 0} \int_{V-V_\epsilon} G_0(\mathbf{x},\mathbf{x}')\nabla'^2 c(\mathbf{x}')dV' = -\lim_{\epsilon\to 0} \int_{V-V_\epsilon} G_0(\mathbf{x},\mathbf{x}')\frac{\rho(\mathbf{x}')}{D_v}dV' = -\int_V G_0(\mathbf{x},\mathbf{x}')\frac{\rho(\mathbf{x}')}{D_v}dV' \tag{A.3}$$

where $\rho(\mathbf{x})$ in the last step is justified, assuming ρ to be non-singular, by noting that the $|\mathbf{x}-\mathbf{x}'|^{-1}$ singularity in $G_0(\mathbf{x},\mathbf{x}')$ is directly integrable in all V. Therefore we just need to consider the limits as $\epsilon \to 0$ of the terms:

$$\begin{aligned}
I^d_{S_\epsilon}(\mathbf{x}) &= \int_{S_\epsilon} c(\mathbf{x}')\partial'_n G_0(\mathbf{x},\mathbf{x}')dS' \\
I^s_{S_\epsilon}(\mathbf{x}) &= \int_{S_\epsilon} G_0(\mathbf{x},\mathbf{x}')\partial'_n c(\mathbf{x}')dS'
\end{aligned} \tag{A.4}$$

we can split the term $I^d_{S_\epsilon}$ as:

$$I^d_{S_\epsilon} = \int_{S_\epsilon} c(\mathbf{x}')\partial'_n G_0(\mathbf{x},\mathbf{x}')dS' = \int_{S_\epsilon} \left[c(\mathbf{x}') - c(\mathbf{x})\right]\partial'_n G_0(\mathbf{x},\mathbf{x}')dS' + c(\mathbf{x})\int_{S_\epsilon} \partial'_n G_0(\mathbf{x},\mathbf{x}')dS' \tag{A.5}$$

The term $\partial'_n G_0(\mathbf{x},\mathbf{x}')$ has a singularity of order 2 for $\mathbf{x}' = \mathbf{x}$, If we assume that $c(\mathbf{x})$ satisfies the Hölder condition:

$$|c(\mathbf{x}) - c(\mathbf{x}')| \leq C|\mathbf{x}-\mathbf{x}'|^\alpha \tag{A.6}$$

for $\mathbf{x}' \in S_\epsilon$ and $\mathbf{x}$ in the neighbourhood of $\mathbf{x}'$, with $C > 0$ and $0 < \alpha \leq 1$, then as $\epsilon \to 0$ the first integral in Eq. (A.5) vanishes.

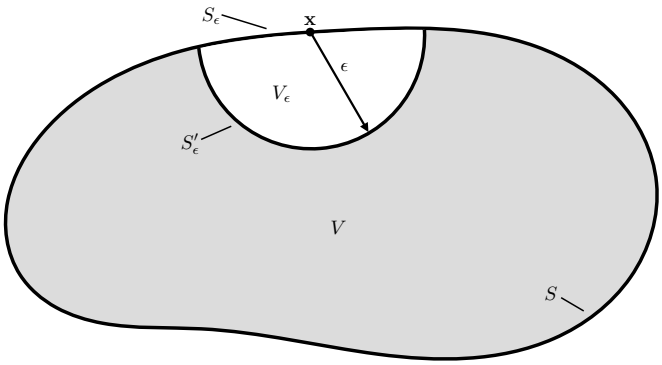

Figure A.8: Schematic diagram of the sets under consideration. The region $V - V_\epsilon$ is shaded in grey.

The second integral can be then straightforwardly computed by taking $\mathbf{x} = 0$ and by noting that:

$$\partial'_n G(0, \mathbf{x}')\Big|_{\mathbf{x}' \in S_\epsilon} = \frac{\partial}{\partial \epsilon} \frac{1}{4\pi D_v \epsilon} = -\frac{1}{4\pi D_v \epsilon^2} \tag{A.7}$$

so that:

$$I^d_{S_\epsilon} = c(\mathbf{x}) \int_{S_\epsilon} \partial'_n G_0(\mathbf{x}, \mathbf{x}') dS' = -\frac{c(\mathbf{x})}{4\pi D_v \epsilon^2} \int_0^{2\pi} d\phi \int_0^{\pi} \epsilon^2 \sin\theta d\theta = -\frac{c(\mathbf{x})}{D_v} \tag{A.8}$$

In a similar way, we can write:

$$\lim_{\epsilon \to 0} I^s_{S_\epsilon}(\mathbf{x}) = -\frac{1}{4\pi D_v} \lim_{\epsilon \to 0} \int_{S_\epsilon} \partial'_n c(\mathbf{x}') dS' = 0 \tag{A.9}$$

which, assuming that there is no point-like source at $\mathbf{x}$, vanishes due the fact that $\partial'_n c(\mathbf{x}')$ is the normal flux of vacancy concentration integrated over a vanishingly small closed surface.
Finally, we obtain the equation:

$$c(\mathbf{x}) = -\int_V G_0(\mathbf{x}, \mathbf{x}') \rho(\mathbf{x}') dV' + D_v \int_S \left[c(\mathbf{x}') \partial'_n G_0(\mathbf{x}, \mathbf{x}') - G_0(\mathbf{x}, \mathbf{x}') \partial'_n c(\mathbf{x}') \right] dS' \tag{A.10}$$

AppendixA.2. Field point on S

Now consider the case where $\mathbf{x} \in S$. Let $B_\epsilon(\mathbf{x})$ be the ball of radius ϵ around $\mathbf{x}$; we define the sets:

$$\begin{aligned} V_\epsilon &= B_\epsilon(\mathbf{x}) \cap V \\ S_\epsilon &= \partial V_\epsilon \cap S \\ S'_\epsilon &= \partial V_\epsilon - S_\epsilon \end{aligned} \tag{A.11}$$

as schematically shown in Fig.A.8. We adapt Eq. (28) to the region $V - V_\epsilon$, bounded by $(S - S_\epsilon) \cup S'_\epsilon$, as:

$$\begin{aligned} \int_V G_0(\mathbf{x}, \mathbf{x}') \frac{\rho(\mathbf{x}')}{D_v} dV' = &\lim_{\epsilon \to 0} \int_{S - S_\epsilon} \left[c(\mathbf{x}') \partial'_n G_0(\mathbf{x}, \mathbf{x}') - G_0(\mathbf{x}, \mathbf{x}') \partial'_n c(\mathbf{x}') \right] dS' + \\ &+ \lim_{\epsilon \to 0} \int_{S'_\epsilon} \left[c(\mathbf{x}') \partial'_n G_0(\mathbf{x}, \mathbf{x}') - G_0(\mathbf{x}, \mathbf{x}') \partial'_n c(\mathbf{x}') \right] dS' \end{aligned} \tag{A.12}$$

where the limiting procedure for volume integrals has already been carried out following the considera-

tions for the case $\mathbf{x} \notin S$, leading to the term on the left hand side. Analogously:

$$\lim_{\epsilon\to 0}\int_{S'_\epsilon} c(\mathbf{x}')\partial'_n G_0(\mathbf{x},\mathbf{x}')dS' = \underbrace{\lim_{\epsilon\to 0}\int_{S'_\epsilon}\left[c(\mathbf{x}')-c(\mathbf{x})\right]\partial'_n G_0(\mathbf{x},\mathbf{x}')dS'}_{=0} + c(\mathbf{x})\lim_{\epsilon\to 0}\int_{S'_\epsilon}\partial'_n G_0(\mathbf{x},\mathbf{x}')dS'. \tag{A.13}$$

Provided that S is smooth[2] , as $\epsilon \to 0$ the surface S_ϵ approaches an hemisphere of radius ϵ centred in $\mathbf{x}$, leading to:

$$c(\mathbf{x})\int_{S'_\epsilon}\partial'_n G_0(\mathbf{x},\mathbf{x}')dS' \to -\frac{c(\mathbf{x})}{4\pi D_v\epsilon^2}\int_0^{2\pi}d\phi\int_0^{\frac{\pi}{2}}\epsilon^2\sin\theta d\theta = -\frac{c(\mathbf{x})}{2D_v} \tag{A.14}$$

Now consider:

$$\lim_{\epsilon\to 0}\int_{S'_\epsilon} G_0(\mathbf{x},\mathbf{x}')\partial'_n c(\mathbf{x}')dS' = -\lim_{\epsilon\to 0}\frac{1}{4\pi D_v\epsilon}\int_{S'_\epsilon}\partial'_n c(\mathbf{x}')dS' \tag{A.15}$$

which vanishes if no source is applied at point $\mathbf{x}$. More generally, even if $\rho(\mathbf{x}) \neq 0$, but provided that it is not singular (i.e. excluding point-like sources), Poisson's equation constrains the possible singular behaviour of $\partial'_n c(\mathbf{x}')$ as:

$$\partial'_n c(\mathbf{x}')\Big|_{\mathbf{x}'\in S_\epsilon} = A\epsilon^{-k} \qquad A\in\mathbb{R},\ 0\le k<1 \tag{A.16}$$

leading to:

$$\lim_{\epsilon\to 0}\frac{1}{4\pi D_v\epsilon}\int_{S'_\epsilon}\partial'_n c(\mathbf{x}')dS' = \lim_{\epsilon\to 0}\frac{1}{4\pi D_v\epsilon}\int_0^{2\pi}d\phi\int_0^{\frac{\pi}{2}}A\epsilon^{-k}\epsilon^2\sin\theta d\theta = \frac{1}{2D_v}\lim_{\epsilon\to 0}\epsilon^{1-k} = 0. \tag{A.17}$$

We are left with a discussion of the terms:

$$\begin{aligned} I^d_{S-S_\epsilon}(\mathbf{x}) &= \int_{S-S_\epsilon} c(\mathbf{x}')\partial'_n G_0(\mathbf{x},\mathbf{x}')dS' \\ I^s_{S-S_\epsilon}(\mathbf{x}) &= \int_{S-S_\epsilon} G_0(\mathbf{x},\mathbf{x}')\partial'_n c(\mathbf{x}')dS' \end{aligned} \tag{A.18}$$

Consider the term $I^d_{S-S_\epsilon}$ and let $r = |\mathbf{x}'-\mathbf{x}|$, we can write:

$$\partial'_n G_0(\mathbf{x},\mathbf{x}') = \frac{\partial G_0(r)}{\partial r}\partial'_n r(\mathbf{x},\mathbf{x}') = \frac{1}{4\pi D_v r^2}\,\partial'_n r(\mathbf{x},\mathbf{x}') = \frac{(\mathbf{x}'-\mathbf{x})\cdot\hat{\mathbf{n}}(\mathbf{x}')}{4\pi D_v r^3} \tag{A.19}$$

but, for $(\mathbf{x}'-\mathbf{x})$ sufficiently small, S can be considered (at least) piecewise flat, thus giving $(\mathbf{x}'-\mathbf{x})\cdot\hat{\mathbf{n}}(\mathbf{x}') = 0$ and cancelling out the singularity for $\mathbf{x}' = \mathbf{x}$. This implies that $\lim_{\epsilon\to 0} I^d_{S-S_\epsilon}(\mathbf{x}) = I^d_S(\mathbf{x})$. Finally, the singularity in $I^s_{S-S_\epsilon}(\mathbf{x})$, of order r^{-1}, can be directly integrated over S. Therefore we obtain the final expression:

$$\frac{c(\mathbf{x})}{2} = -\int_V G_0(\mathbf{x},\mathbf{x}')\rho(\mathbf{x}')dV' + D_v\int_S\left[c(\mathbf{x}')\partial'_n G_0(\mathbf{x},\mathbf{x}') - G_0(\mathbf{x},\mathbf{x}')\partial'_n c(\mathbf{x}')\right]dS' \tag{A.20}$$

[2] As a matter of fact, we can relax this assumption. In the general case the result of eq.A.14 is given by $-\frac{\alpha(\mathbf{x})c(\mathbf{x})}{4\pi D_v}$, where $\alpha(\mathbf{x})$ is the solid angle of the infinitesimal surface element of S at point $\mathbf{x}$.

[1] Y. Gu, Y. Xiang, S. S. Quek, D. J. Srolovitz, Three-dimensional formulation of dislocation climb, Journal of the Mechanics and Physics of Solids (2015) 1–19.
[2] F. París, J. Cañas, Boundary Element Method, Fundamentals and Applications, 1st Edition, Oxford University Press, 1997.
[3] F. Ferroni, X. Yi, K. Arakawa, S. P. Fitzgerald, P. D. Edmondson, S. G. Roberts, High temperature annealing of ion irradiated tungsten, Acta Materialia 90 (2015) 380–393.
[4] E. E. Bloom, Structural materials for fusion reactors, Nuclear Fusion 30 (9) (1990) 1879–1896.
[5] W. Van Renterghem, I. Uytdenhouwen, Investigation of the combined effect of neutron irradiation and electron beam exposure on pure tungsten, Journal of Nuclear Materials 477 (2016) 77–84.
[6] K. Fukumoto, M. Iwasaki, Q. Xu, Recovery process of neutron-irradiated vanadium alloys in post-irradiation annealing treatment, Journal of Nuclear Materials 442 (1-3 SUPPL.1) (2013) 360–363.
[7] T. Nagasaka, T. Muroga, H. Watanabe, K. Yamasaki, K. Heo, N.-J.and Shinozaki, M. Narui, Recovery of Hardness, Impact Properties and Microstructure of Neutron-Irradiated Weld Joint of a Fusion Candidate Vanadium Alloy 46 (3) (2005) 498–502.
[8] T. S. Byun, J. H. Baek, O. Anderoglu, S. A. Maloy, M. B. Toloczko, Thermal annealing recovery of fracture toughness in HT9 steel after irradiation to high doses, Journal of Nuclear Materials 449 (1-3) (2014) 263–272.
[9] M. Rieth, S. L. Dudarev, S. M. Gonzalez De Vicente, J. Aktaa, T. Ahlgren, S. Antusch, D. E. J. Armstrong, M. Balden, N. Baluc, M. F. Barthe, W. W. Basuki, M. Battabyal, C. S. Becquart, D. Blagoeva, H. Boldyryeva, J. Brinkmann, M. Celino, L. Ciupinski, J. B. Correia, A. De Backer, C. Domain, E. Gaganidze, C. García-Rosales, J. Gibson, M. R. Gilbert, S. Giusepponi, B. Gludovatz, H. Greuner, K. Heinola, T. Höschen, A. Hoffmann, N. Holstein, F. Koch, W. Krauss, H. Li, S. Lindig, J. Linke, C. Linsmeier, P. López-Ruiz, H. Maier, J. Matejicek, T. P. Mishra, M. Muhammed, A. Muñoz, M. Muzyk, K. Nordlund, D. Nguyen-Manh, J. Opschoor, N. Ordás, T. Palacios, G. Pintsuk, R. Pippan, J. Reiser, J. Riesch, S. G. Roberts, L. Romaner, M. Rosiński, M. Sanchez, W. Schulmeyer, H. Traxler, A. Ureña, J. G. Van Der Laan, L. Veleva, S. Wahlberg, M. Walter, T. Weber, T. Weitkamp, S. Wurster, M. A. Yar, J. H. You, A. Zivelonghi, Recent progress in research on tungsten materials for nuclear fusion applications in Europe, Journal of Nuclear Materials 432 (1-3) (2013) 482–500.
[10] D. Bacon, T. Diaz de la Rubia, Molecular dynamics computer simulations of displacement cascades in metals, Journal of Nuclear Materials 216 (C) (1994) 275–290.
[11] N. M. Ghoniem, Theory of microstructure evolution under fusion neutron irradiation, Journal of Nuclear Materials 179-181 (PART 1) (1991) 99–104.
[12] S. L. Dudarev, Inhomogeneous nucleation and growth of cavities in irradiated materials, Physical Review B 62 (14) (2000) 9325–9337.
[13] K. Arakawa, K. Ono, M. Isshiki, K. Mimura, M. Uchikoshi, H. Mori, Observation of the one-dimensional diffusion of nanometer-sized dislocation loops., Science (New York, N.Y.) 318 (5852) (2007) 956–959.
[14] S. L. Dudarev, M. R. Gilbert, K. Arakawa, H. Mori, Z. Yao, M. L. Jenkins, P. M. Derlet, Langevin model for real-time Brownian dynamics of interacting nanodefects in irradiated metals, Physical Review B - Condensed Matter and Materials Physics 81 (22) (2010) 1–15.
[15] S. L. Dudarev, K. Arakawa, X. Yi, Z. Yao, M. L. Jenkins, M. R. Gilbert, P. M. Derlet, Spatial ordering of nano-dislocation loops in ion-irradiated materials, Journal of Nuclear Materials 455 (1-3) (2014) 16–20.
[16] B. Bakó, E. Clouet, L. Dupuy, M. Blétry, Dislocation dynamics simulations with climb: kinetics of dislocation loop coarsening controlled by bulk diffusion, Philosophical Magazine 91 (21) (2011) 3173–3191. arXiv:1401.6784.
[17] D. Mordehai, E. Clouet, M. Fivel, M. Verdier, Introducing dislocation climb by bulk diffusion in discrete dislocation dynamics, Philosophical Magazine 88 (6) (2008) 899–925.
[18] Y. Xiang, L.-T. Cheng, D. Srolovitz, W. E, A level set method for dislocation dynamics, Acta Materialia 51 (18) (2003) 5499–5518.
[19] Y. Xiang, D. Srolovitz, Dislocation climb effects on particle bypass mechanisms, Philosophical Magazine 86 (25-26) (2006) 3937–3957.
[20] K. M. Miller, P. T. Heald, The lattice distortion around a vacancy in F.C.C. metals, Physica Status Solidi (B) 67 (2) (1975) 569–576.
URL http://dx.doi.org/10.1002/pssb.2220670219
[21] F. Hofmann, D. Nguyen-Manh, M. R. Gilbert, C. E. Beck, J. K. Eliason, A. A. Maznev, W. Liu, D. E. J. Armstrong, K. A. Nelson, S. L. Dudarev, Lattice swelling and modulus change in a helium-implanted tungsten alloy: X-ray micro-diffraction, surface acoustic wave measurements, and multiscale modelling, Acta Materialia 89 (2015) 352–363.
URL http://dx.doi.org/10.1016/j.actamat.2015.01.055
[22] S. L. Dudarev, Density Functional Theory Models for Radiation Damage, Annual Review of Materials Research 43 (1) (2013) 35–61.
[23] J. Hirth, J. Lothe, Theory of dislocations, 2nd Edition, Wiley, New York, 1982.
[24] M. R. Gilbert, S. L. Dudarev, P. M. Derlet, D. G. Pettifor, Structure and metastability of mesoscopic vacancy and interstitial loop defects in iron and tungsten, Journal of Physics: Condensed Matter 20 (34) (2008) 345214.
[25] D. N. Beshers, On the Distribution of Impurity Atoms in the Stress Field of a Dislocation, Acta Metallurgica 6 (August) (1958) 521–523.
[26] X. Yi, M. Jenkins, M. Briceno, S. Roberts, Z. Zhou, M. Kirk, In situ study of self-ion irradiation damage in W and W–5Re at 500 °C, Philosophical Magazine 93 (14) (2013) 1715–1738.
[27] T. Amino, K. Arakawa, H. Mori, Activation energy for long-range migration of self-interstitial atoms in tungsten obtained by direct measurement of radiation-induced point-defect clusters, Philosophical Magazine Letters 91 (2) (2011) 86–96.